AN INVESTIGATION INTO METHODS OF DETECTING DEWETTED ZONES IN SOLID ROCKET PROPELLANTS USING HOLOGRAPHIC INTERFEROMETRY

Donald Arthur Hallwachs

NAVAL POSTGRADUATE SCHOOL
Monterey, California

THESIS

AN INVESTIGATION INTO METHODS OF DETECTING DEWETTED ZONES IN SOLID ROCKET PROPELLANTS USING HOLOGRAPHIC INTERFEROMETRY

by

Donald Arthur Hallwachs

Advisor: G. H. Lindsey

June 1973

Approved for public release; distribution unlimited.

An Investigation into Methods of Detecting Dewetted Zones in Solid Rocket Propellants Using Holographic Interferometry

by

Donald Arthur Hallwachs
Lieutenant, United States Navy
B.S., United States Naval Academy, 1965
M.S., Naval Postgraduate School, 1972

Submitted in partial fulfillment of the
requirements for the degree of

AERONAUTICAL ENGINEER

from the

NAVAL POSTGRADUATE SCHOOL
June 1973

ABSTRACT

An investigation was conducted into the possibility of visually detecting a dewetted zone in a solid rocket propellant through the use of holographic interferometry. Techniques used were simple strain, residual strain and time-average holography. As a basis for comparison with experimental data a finite element program was used to model the test samples.

TABLE OF CONTENTS

I. INTRODUCTION

A. DEWETTING

Dewetting is the phenomenon that makes filled materials (rocket propellants) differ from classical viscoelastic (unfilled) materials. Propellant consists of a composite of solid oxidizer particles imbedded in and bonded to a fuel matrix. After an initial linear region, nonlinear stress-strain behavior under loading results from the progressive failure of these bonds at the interface between the fuel matrix and the oxidizer particles. Voids or vacuoles are thus created throughout the materials and their volume increases with further loading, causing an overall volume increase in the material. This phenomenon is called dewetting.

B. DEWETTING THEORY

Lindsey [1] has postulated that a dewetting criterion exists and that it is expressible as

$$J_2 + \alpha(I_1)^2 = \text{constant}$$

where J_2 is the second deviatoric stress invariant, I_1 the first stress invariant and α is a small constant. This expression represents a surface in principle stress space that is axisymmetric about the hydrostatic axis ($\sigma_1 = \sigma_2 = \sigma_3$). Figure 1 is a sketch of the general shape of this surface. A state of stress located outside of or on this surface will be dewetted.

C. EVALUATION OF THEORY

The dewetting created by excess strain is not visible to the naked eye. However, changes in the dewetted material properties will result in a displacement field that is different from that of a material which has similar properties but does not dewet. To test the postulate of Lindsey, holographic interferometry was selected to detect these displacement changes because (1) it is sensitive to very small displacements and (2) holography models need not be transparent and birefringent as in the case of photoelasticity.

Attempts to identify a dewetted area through the visual interpretation of the interferometric fringe patterns include the techniques of small strains, residual strains and vibrational time average.

A finite element program was used as a basis of comparison between the displacements obtained holographically from both dewetting and nondewetting materials of similar shape undergoing small strains.

II. EXPERIMENTAL APPARATUS

A. THE HOLOGRAPHIC SETUP

The holographic setup was of a conventional nature. An airtable was used consisting of a two-inch thick piece of plywood, four by eight feet in dimensions, supported by four inner tubes resting on a heavy metal table. Very good vibration insulation was obtained.

A Spectra-Physics 15 milliwatt continuous wave helium-neon laser beam was expanded through a spatial filter and directed onto the sample. A front surface mirror was mounted beside the sample to provide a reference beam. The path length from source to sample to holographic plate was approximately the same as the path length from source to reference mirror to plate. The holographic plate was mounted directly in front of the sample. Figure 2 is a schematic and photograph of the setup.

The film used was Agfa-Gevaert 8E75 Scientia four-by-five inch plates. The developing procedure was five minutes in Kodak D-19 developer, 30 seconds in a stop bath and five minutes in a fixer followed by a 30-minute water bath.

B. THE TENSILE TESTING MACHINE

The use of a conventional tensile testing machine was rejected because it has only one moving crosshead. Straining a sample from one end results in the center of the sample moving about half the distance of the crosshead.

This movement is undesirable in holographic work where even pure rigid body movement causes fringes in double exposure interferograms.

To minimize the translation of the center of the sample, a tensile testing machine was built that had two moving crossheads. Turning the handwheel resulted in the crossheads moving in opposite directions. One complete turn of the handwheel resulted in each crosshead moving 0.005 inch. Figure 3 is a photograph of the machine.

The handwheel had notches in it every five degrees which engaged a springwire latch. This allowed the handwheel to be turned in multiples of five degrees in the dark for double exposure work.

C. THE TEST SAMPLES

The test samples were six-by-six inch squares, one-quarter inch thick, with a one-inch diameter hole in the center to act as a stress riser. A one-inch piece of wood was bonded to two sides of the samples to provide a place for mounting in the tensile testing machine. This type of geometry was selected for its ease of construction and its two-dimensional plane stress properties.

The sample material was obtained from United Technology Corporation, Sunnyvale, California. The unfilled material was rocket motor case liner of type C-296-182-7 and the filled material was rocket propellant of type UTP-3001. Figure 4 is a drawing of the sample geometry.

III. DISPLACEMENT FIELD DETERMINATION

A. COMPUTER GENERATED DISPLACEMENTS

1. The Finite Element Program

As a basis for comparison with the experimental data a finite element program called PSELST (Plane Stress Elastic Analysis Using Linear Strain Triangles) was used to model the test samples. This program was able to handle plane stress problems with up to six different types of material in its composition. This is a necessary feature in order to handle the material property changes caused by dewetting. The outputs of the program were the stresses and displacements at each node in the model. Reference 2 describes PSELST in great detail.

2. The Finite Element Grid

The finite element grid is shown in Figures 5 and 6. Only the upper right-hand quadrant of the sample was modeled due to the symmetry of the sample and of the loading. The smaller elements were placed around the hole where the stress gradients would be the highest. The origin of the grid coordinate system was placed at the center of the hole with the X-axis as the horizontal lower boundary and the Y-axis as the vertical left hand boundary.

3. The Boundary Conditions

The boundary conditions on the problem were straightforward. Nodal points on the X-axis were free to slide in the plus or minus X-direction only and the nodal points on

the Y-axis were free to move in the plus or minus Y-direction only. Nodal points along the upper boundary were all given a uniform positive Y displacement with no X displacement to simulate a crosshead moving up and straining the sample. The right edge nodal points were a free boundary.

4. The Unfilled Material Solution

The material properties for the unfilled sample were taken to be 470 psi for the elastic modulus and 0.485 for Poisson's ratio, which are typical values for this type of material. Experiments have shown that this material is linear to about fifteen percent strain. For this reason it was assumed for the computer solution that the modulus of elasticity and Poisson's ratio were constants.

It can be shown that for a displacement boundary condition problem, the value of the elastic modulus does not affect the resultant displacement field if Poisson's ratio is held constant. As a sensitivity test, two computer displacement solutions were obtained, one with a modulus of 470 psi and the other with a modulus of 1090 psi. Both had a Poisson's ratio of 0.485. The resultant displacement fields agreed to within 0.0003 wave lengths of light for a boundary extension of 18.906 wave lengths.

A second sensitivity test was conducted with the elastic modulus held constant at 470 psi and Poisson's ratio set at 0.485 for the first run and 0.495 for the second. The change in the displacement field was small and probably

within the error range of the holographic technique. For example, for a boundary extension of 24.136 wave lengths of light, the difference between the predicted X displacements was 0.0579 wave lengths at grid point 33.

The results of the sensitivity tests indicated that the computer displacements for the unfilled material were unaffected by an elastic modulus change of every element if Poisson's ratio was held constant and that the solution was relatively insensitive to a Poisson's ratio change of every element if the elastic modulus was held constant.

5. The Filled Material Solution

The modulus of elasticity for the filled material was obtained from a uniaxial tensile test. (Figure 7). The stress-strain curve was linearized by dividing it into four segments and replacing each segment with a straight line. Poisson's ratio for the filled material was estimated from data obtained by Lindsey and Wood [1]. Table I is a summary of the data. The departure of the stress-strain curve from linearity is due to the onset of dewetting and the stress at that point, σ_o , is called the yield or dewetting stress.

The first segment of the curve starting at zero stress was considered the nondewetted portion and was designated material of type one. Type two material, which was partially dewetted, was represented by the second segment of the curve. Type three was dewetted to a greater degree and type four was considered to be completely dewetted.

The upper end of the fourth segment was the stress, σ_{max}, at which probable failure of the material would occur.

To relate the two-dimensional stress of the computer solution to the one-dimensional stress-strain curve, an equivalent stress σ_e was used. Equivalent stress [3] is defined as

$$\sigma_e = \sqrt{3J_2}$$

$$J_2 = \frac{1}{6}\left[(\sigma_x-\sigma_y)^2+(\sigma_x-\sigma_z)^2+(\sigma_y-\sigma_z)^2 + 6(\tau_{xy}^2+\tau_{xz}^2+\tau_{yz}^2)\right]$$

For plane stress

$$\sigma_z = \tau_{xz} = \tau_{yz} = 0$$

Thus

$$\sigma_e = (\sigma_x^2 + \sigma_y^2 - \sigma_x\sigma_y + 3\tau_{xy}^2)^{1/2}$$

This equivalent stress was used because the value of α has been found to be very small for this type of material. For typical values of α and the stress field of the specimen, the dewetting criterion and the equivalent stress agree to within one percent.

For the computer solution the upper edge was extended 0.01 inches at a time. Although the overall properties are nonlinear, each 0.01 inch step was considered small enough to be linear. After each extension, the output stresses σ_x, σ_y and τ_{xy} at each node were used to determine the equivalent stress at that node. If the equivalent

stress was less than σ_o , the node was considered to still be of material type one. When the equivalent stress fell within the range of segment two, the node was considered to be material of type two and so on. When the equivalent stress exceeded σ_{max} , failure was probable at that node. Each quadrilateral finite element had nine nodes associated with it, but only four were nodal points in the grid. The program, internal to itself, added a node to the midpoint of each side and at the intersection of the element's diagonals. It was decided that whenever any two of the element's nine nodes, six in the case of a triangular element, had changed to the next higher material type, then the element itself would be changed to that next higher material type. Once an element or node reached material type four it remained type four.

Originally the criterion was that five of nine nodes had to change to the next highest material type before an element was changed to that type. This resulted in a rapid stress buildup at node one and failure was predicted after only 0.11 inch of upper edge extension. Thus a less stringent element changing criterion was adopted in an attempt to relieve the stress buildup at node one, because it was known from experiments that the actual samples did not fail until 0.225 inches of extension.

In addition to checking for material changes, the incremental nodal displacements were added to the nodal coordinates to obtain the new coordinates for the next extension.

The incremental procedure used to extend the computer solution to 0.20 inches may be summarized as the following iterative routine:

a. Extend the upper boundary 0.01 inch.

b. Add the incremental stresses to a running total of stresses from the previous extensions.

c. Compute the nodal equivalent stresses based on the summation of stresses and assign each node its proper material type based on the linearized stress-strain curve.

d. Check each element to see if any two of its nodes have changed to the next higher material type. If yes, change that element's properties to the next higher type.

e. Add the incremental displacements to the nodal coordinates to form the new nodal coordinates for the next incremental extension.

f. Return to step a.

Using the above technique, failure was predicted to occur at node one after only 0.12 inches of upper edge extension. It was known that the samples were extended to 0.225 inches before actual failure, so the computer prediction of failure was ignored and the solution continued on to 0.20 inches of extension.

If the dewetting criterion is applied to the classical solution for the stress field around a hole in an infinite sheet, the outline of the dewetted zone will be as shown in Figure 8. For comparison, the computer solution for the dewetted zone in the filled material using equivalent stress is shown for 0.13 inches of extension in Figure 9.

6. Nondimensional Displacements

The X and Y displacements obtained from PSELST were due to a 0.01 inch extension of the upper edge. However, the unfilled material was considered linear so that displacements for extensions other than 0.01 were obtained by scaling.

Predicting displacements for the filled material was more restrictive. The displacements had to be scaled from the X and Y displacements of the twentieth step of the incremental routine.

All displacements were nondimensionalized by dividing by the wave length of light from the Helium-Neon Laser.

B. DISPLACEMENTS BY HOLOGRAPHIC MEANS

1. Holographic Displacement Theory

The method presented here was developed by S.K. Dhir and J.P. Sikora [4]. If a light-scattering object undergoes an elastic deformation between two holographic exposures constituting the interferogram, the fringes will be related to the displacement field. Let the point P(X,Y,Z) be displaced to P'(X+u,Y+v,Z+w) where u, v and w are the cartesian components of the displacement vector (Figure 10). Points H(Xk,Yk,Zk) and S(Xo,Yo,Zo) are the observation points on the hologram plate and the light source respectively. The total distance traveled by the light will be (SP+PH) before movement and (SP'+P'H) after movement. The difference in

path lengths can be expressed as some multiple of the wave length of the laser light, L,

$$nL = (SP'+P'H) - (SP+PH) \tag{1}$$

where n is any number. If n is a whole number then the object point will appear bright because the two waves will be in phase. If n is some odd multiple of 1/2 then the waves will arrive out of phase and the object point will appear dark.

$$\begin{aligned} SP' &= [(X-Xo+u)^2+(Y-Yo+v)^2+(Z-Zo+w)^2]^{1/2} \\ SP &= [(X-Xo)^2+(Y-Yo)^2+(Z-Zo)^2]^{1/2} \\ P'H &= [(X-Xk+u)^2+(Y-Yk+v)^2+(Z-Zk+w)^2]^{1/2} \\ PH &= [(X-Xk)^2+(Y-Yk)^2+(Z-Zk)^2]^{1/2} \end{aligned} \tag{2}$$

Rearrange equation (1)

$$nL = (SP'-SP)+(P'H-PH) \tag{3}$$

Substitute (2) into (3) and the first term becomes

$$SP' = SP\left[\, 1 + \frac{1}{(SP)^2}\left\{ 2[(X-Xo)u + (Y-Yo)v + (Z-Zo)w] + u^2 + v^2 + w^2 \right\}\right]^{1/2}$$

Neglecting small quantities in the expansion of SP' it can be shown that

$$(SP'-SP) = \frac{1}{SP}\left[\, (X-Xo)u + (Y-Yo)v + (Z-Zo)w \,\right] \tag{4}$$

The distance (P'H - PH) can be found by replacing the subscript o with k and 1/SP with 1/PH.

Now

$$n_kL = A_ku + B_kv + C_kw \tag{5}$$

Where

$$A_k = \frac{X-Xo}{SP} + \frac{X-Xk}{PH}$$

$$B_k = \frac{Y-Yo}{SP} + \frac{Y-Yk}{PH} \qquad (6)$$

$$C_k = \frac{Z-Zo}{SP} + \frac{Z-Zk}{PH}$$

The subscript k refers to a single point of observation on the holographic plate (Figure 11) and n_k is the respective fringe number on the point being observed.

The same object point can be observed through three different points on the plate. The result is three equations in three unknowns which can be solved for u, v, and w.

If it is not possible to determine the location of the zero order fringe, Equation (5) is modified to

$$(n_k-n_{k+1})L = (A_k-A_{k+1})u + (B_k-B_{k+1})v + (C_k-C_{k+1})w \qquad (7)$$

where (n_k-n_{k+1}) is the number of fringes that shift through an object point going from position k to k+1 on the plate. When this subtraction is carried out, all the terms involving 1/SP drop out. Thus when using these equations with an unknown zero order fringe the location of the source is unimportant. This eliminates errors in determining the physical coordinates of the source. This advantage is offset by the necessity of combining two observations of the same point to determine one equation. The sign assigned to a fringe shift is not important as long as the system used is consistent.

In theory it should take only three observations to determine the three unknowns. However, the value of the

determinant of these equations is very small due to the limited size of the plate. With only three equations large errors can be expected. The errors can be greatly reduced if more than three equations are generated for each object point, and a linearly overdetermined least squares method is used to solve them. Subroutine LLSQ in the IBM library was used. Nine equations were used to determine the three unknown displacements.

The accuracy of the measurements of the physical set-up was within 0.1 inch and the accuracy of the fringe count was estimated to be $\pm$ 0.1 fringe number. See Table II for a sensitivity test.

A further refinement of Equation (7) is to divide through by L. The three unknowns then become nondimensional displacements.

$$U = \frac{u}{L} \ , \ V = \frac{v}{L} \ , \ W = \frac{w}{L}$$

Thus, even if the wave length of the laser is unknown, a relative displacement field can be obtained.

The displacement vector obtained from LLSQ may or may not have to be multiplied by (-1). The sign of the displacement vector cannot be determined from holographic measurements alone because the reconstructed image and the direction of fringe movement remains unaffected even if the direction of the displacement vector is reversed by reversing the sequence of the two exposures. A priori knowledge about the direction of at least one displacement component is therefore necessary in order to assign proper signs to the other two components.

If the fringe distortion about a point is severe, there may be larger than 0.1 fringe count errors. A technique proposed by Dhir to detect this involves plotting fringe difference, $(n_k - n_{k+1}) = \Delta n$, along a given cross section of the object. A deformed object should show continuous and smooth fringe differences. If the plots of Δn are not smooth, a smooth curve is passed through the data. In this way the Δn for a distorted fringe area can be obtained with more accuracy.

2. The Unfilled Sample Experiment

The sample was extended to 0.135 inches and allowed to relax for more than one-half hour. The first exposure was then made and the wheel was turned forty degrees to make the second exposure (Figure 12). It was found by experiment that for these samples a forty-degree turn of the wheel produced the best fringe density. A larger turn resulted in the fringes being too close for accurate counting. A smaller turn produced fringes that were too broad and increased the difficulty of estimating the fringe number at a point.

Nine viewing ports were drawn on the holographic plate with india ink and numbered one through nine. (See Figure 11).

The location of the zero order fringe was unknown, so two observations of a single grid point had to be combined to produce one equation. Each grid point was observed nine times to ensure enough over-determination for the least squares computer solution. The nine viewing ports

were used in the following combinations for each point: 1-7, 1-8, 1-9, 2-7, 2-8, 2-9, 3-7, 3-8, 3-9 or 1-3, 1-6, 1-9, 4-3, 4-6, 4-9, 7-3, 7-6, 7-9. If certain combinations were unreadable, variations on the above were used.

For example, when determining the fringe difference for set 1-7, the object grid point would be sighted through port number one and assigned an arbitrary fringe number. If the grid point viewed through port one was half way between two dark fringes, it would be assigned a fringe number of 0.5. The line of sight was then slowly changed to viewport seven while keeping count of how many fringes passed over the grid point. If the grid point when viewed through port seven was between fringes three and four, then the number 3.5 would be assigned. For purposes of the LLSQ solution, the fringe difference would be 3.0. The actual tenth of a fringe number assigned for each point was determined by visual interpolation between centers of dark fringes. Most of the fringes could be readily estimated to plus or minus one-tenth of a fringe. For crowded or severely distorted fringes this was not always possible. This is why the fringe-difference curve smoothing was used.

In addition to the 59 grid points used there were seven defined points on each crosshead to provide a reference for the determination of rigid body displacements and the true extension of the sample.

The smoothed data were used to solve for the total U,V, and W of each grid point. The U, V, and W obtained

consisted of two parts, the displacement relative to the axis system and the displacement due to rigid body affects. Thus:

$$U = Ud + Urb$$
$$V = Vd + Vrb$$
$$W = Wd + Wrb$$

The subscript d refers to displacements relative to the axes. This is the quantity desired for comparison with the computer solution. The subscript rb refers to the rigid body displacement. The rigid body displacements were determined and subtracted from the total displacements to yield the relative displacements.

The rigid body displacements of the sample were determined from the displacement of the X and Y axes. It was assumed that the X and Y axes remained straight even under stress due to the geometric symmetry. Therefore, any V displacement along the X-axis was due completely to rigid body displacement. Any U displacement along the Y-axis was due completely to rigid body displacement. That is, U = Urb along the Y-axis and V = Vrb along the X-axis.

As stated previously, a priori knowledge of one displacement component must be known before the proper sign can be given to the other two components. It was known that the V displacements of the nodal points on the Y-axis were positive since that was the sign of the upper crosshead extension. Therefore the sign of the U and W displacements was also determined for the Y-axis. A linear least squares curve was fitted through the U displacements, making Urb a

function only of Y. It was then assumed that the Urb displacement of any point on the body was a function of its Y coordinate only.

By letting Y equal zero, the Urb for points on the X-axis was determined. Although Ud along the X-axis was unknown its sign was known to be negative from the Poisson effect of a positively strained body. Therefore,

$$U - Urb \leq 0$$

and in addition Ud must become more negative as the X distance from the origin increases.

As an example, the following is a sample of the data obtained for two nodal points on the X-axis. (Figure 6)

Point	U	V	W
3	8.2512	3.8745	30.7820
6	11.2715	4.0733	28.3705

All the values are positive but it was not known whether they should be. It was determined using the method described that Urb for the X-axis was -2.5057. Applying the formula to point three,

$$\pm 8.2512 - (-2.5057) \leq 0$$

shows that the U for point three must be negative and therefore U and W are also negative. Then Ud3 = -5.7455 and Ud6 = -8.7658 and the second requirement is met. With the Vrb for the X-axis known to be negative, these points were also fitted with a linear least squares curve and it was assumed that the Vrb of any point was a function of its X coordinate only.

The determination of Wrb is very difficult and can only be approximated at best. There are no sections of the sample that can be assumed to remain straight for displacements in the Z direction. In addition, the maximum Wd displacement was predicted from the computer solution to be only on the order of two wave lengths with most points being on the order of one or less, which borders on the expected accuracy limits of the fringe count displacement prediction method. For this reason W was not considered in the comparisons of displacements.

As a point of interest, it was noted during the counting of fringes that the maximum fringe shift would occur if the observation viewports used were in a line parallel to the maximum displacement component.

For the unfilled material experiment the additional extension of the upper end was found to be 24.7041 wave lengths of light. Forty degrees of handwheel turn was expected to cause 22.3 wave lengths of additional extension.

3. The Filled Sample Experiment

The methods used to make the interferograms and obtain the data for the filled sample were identical to those of the unfilled sample. The only change was in the amount of extension given the filled sample prior to the making of the interferogram. It was found by experiment that the samples would fail by cracking when the extension was about 0.225 inches. The sample was extended to 0.20 inches to ensure

that dewetting would take place. Figure 13 is a photograph of the fringe pattern obtained.

For the filled material experiment the additional extension of the upper edge was found to be 18.9060 wave lengths of light.

IV. OTHER METHODS

A. SIMPLE EXTENSION

The simplest method attempted was to apply a small extension between exposures and visually search for anomalies in the fringe pattern. No such pattern was detected which could be attributed to a dewetted zone. Figure 13 is a typical example of a fringe pattern obtained. Unwanted rigid body motion may have caused fringe patterns which disguised the zone.

B. RESIDUAL STRAIN

The residual strain method makes use of material property changes. The object was photographed at one state of strain and then the crosshead was extended another 0.005 inch. The increased strain caused more of the sample to dewet. The crosshead was then returned to its original position and the second exposure made. The material that changed properties between exposures will not be able to return to its original state and this will cause fringes. Figures 14 and 15 are examples of this technique. The resulting fringe patterns vary widely. On several occasions, patterns appeared in one or more quadrants that may or may not have been dewetted zones. Fringe patterns on the crossheads indicated that they were not returned to exactly the original extension and/or that rigid body motion had taken place between exposures.

C. TIME AVERAGE

Samples of the filled material were acoustically excited and time average holograms were made. The range of excitation frequencies used was from 60 to 1000 cycles per second. The holograms obtained showed no indication of a dewetted area. (Figure 16)

V. RESULTS AND CONCLUSIONS

A. THE UNFILLED MATERIAL

The computer-predicted displacements and the measured displacements for the unfilled material are plotted versus radial distance for each ten-degree radial of the finite element grid. (Figures 17 through 21). An examination of the plots indicates that the linear theory does not accurately predict the behavior of the sample. The measured U and V displacements are higher than predicted on every radial.

There are indications that the deviation from linearity depends upon the intensity of the stress. It can be seen that the V measured points match very well with the shape of the V predicted curve at the higher radials. Since the displacement at any point is the integral of the strains up to that point, it would indicate that the material at the higher radials is behaving linearly and the larger than predicted displacements are due to the nonlinear strains on the lower radials.

Another unexpected result is that the measured U for the ten-degree radial is larger than that of the zero-degree radial. The U for the 20-degree radial is smaller than the U for the 10-degree radial but still larger than the zero. It is not until the 30-degree radial that the measured U is smaller than that of the zero-degree radial. The predicted

U is greatest for the zero-degree radial and decreases for each increase in radial.

B. THE FILLED MATERIAL

For the filled material the linear predictions, the dewetted predictions and the measured displacements are plotted versus radial distance for each radial. (Figures 22 through 26).

The linear V displacements predictions were in general better than the dewetted predictions. This is due in part to the early prediction of failure from the dewetted program. The failure prediction was discounted and the result was that the predicted dewetted zone grew to cover most of the right-hand side of the grid. The lowered elastic moduli of the dewetted lower radials allowed too much strain to occur in the elements along the X-axis, with the resultant larger displacements at the higher radials.

Both computer methods underestimate the U displacements and they agree with each other very well for the 30-degree radial and higher.

The measured values of V fell between the linear and dewetted computer solutions but were closer to the linear solution. This indicates that the material did dewet but to a much smaller extent than predicted by theory.

C. FILLED DISPLACEMENTS COMPARED WITH UNFILLED DISPLACEMENTS

The measured displacements for the filled and unfilled material are plotted versus radial distance for each ten

degree radial (Figures 27 through 31). The unfilled displacements were converted to the same upper edge extension as the filled material by multiplying by

$$\frac{18.9060}{24.7041} = 0.765298$$

The unfilled displacements are greater than the filled displacements for every radial but in general the shapes of the displacement curves are similar. This appears to be due to nonlinear straining of the unfilled material in the lower radials.

D. THE HOLOGRAPHIC DISPLACEMENT DETERMINATION METHOD

The method for obtaining general displacements from a holographic interferogram proved to be simple to understand and easy to use. However, its use is not recommended for general use because of the large amount of time that must be spent to obtain data. It is estimated that a total of twelve hours were spent just to determine the nine fringe differences for each of the 73 points used in the analysis.

E. THE TENSILE MACHINE

The tensile machine, as designed, was not rigid enough. The unwanted movement of the machine induced fringe patterns onto the sample that disguised the true patterns and made simple visual inspection of the patterns impossible. Any continuation of this work should be done with a much more rigid tensile testing machine.

F. EQUIVALENT STRESS

The concept of equivalent stress was derived for use in predicting plasticity in metals. It is used to relate a three-dimensional stress state to a one-dimensional one such as a stress-strain diagram, however it is only a postulate, not a proven fact. The effects of plasticity and dewetting, as far as the stress-strain diagrams are concerned, are the same so it seemed a logical extension of the equivalent stress idea to apply it to dewetting of propellants. The results indicate that this is not the case and that equivalent stress may not be applied to dewetting with accurate results.

G. THE FINITE ELEMENT PROGRAM

From the inaccuracy of the computer displacement predictions and the early prediction of propellant sample failure it is evident that a finite element material property change criterion based on equivalent stress alone will not give satisfactory results. The effects of viscoelastic stress relief will have to be incorporated into the computer dewetting criterion so that stresses will build more slowly without over-predicting the resultant displacements.

The linear finite element program more closely predicted the V displacements of the propellant but it also predicted a stress of over 200 psi at node one for a 0.20 inch extension,

which is over twice the failure stress obtained from the tensile test. The sample did not fail at 0.20 inches of extension which emphasizes the importance of viscoelastic stress relief incorporation into the finite element model.

H. CONCLUDING REMARKS

The comparison of the computer predicted displacements to the measured data was unsuccessful due to the inconsistency of the results. Modifications to the computer technique as discussed in section G should produce better results. In addition, a more rigid tensile testing machine would eliminate errors resulting from rigid body motion and unsymmetric crosshead extension.

The dewetted zone was not detected visually. The most promising technique appears to be the residual strain method and further investigation of the technique is recommended.

TABLE I

TABULATION OF MATERIAL PROPERTIES

MATERIAL TYPE	POISSON'S RATIO	ELASTIC MODULUS
1	0.485	1091.0
2	0.483	905.7
3	0.481	754.7
4	0.480	294.3

TABLE II

TEST of SENSITIVITY of LEAST SQUARES FRINGE DIFFERENCE METHOD

Data used:

Object Number	First View Port	Second Port	Δn
1	1	3	3.7
1	1	6	3.8
1	1	9	3.1
1	4	3	4.0
1	4	6	4.1
1	4	9	3.4
1	7	3	4.3
1	7	6	4.4
1	7	9	3.7

Test results:

Number of Equations used	Solution U	V	W	
4	-7.633	-3.172	-19.69	
5	-7.637	-3.437	-21.83	
6	-7.875	-3.020	-17.27	
7	-7.894	-2.489	-14.38	
8	-7.896	-2.542	-15.07	
9	-7.829	-2.544	-15.07	
9	-7.799	-2.550	-15.19	note (1)
9	-8.053	-2.544	-15.08	note (2)
9	-7.605	-2.544	-15.06	note (3)

Note (1) Odd numbered data cards had 0.1 subtracted from Δn and even numbered cards had 0.1 added.

Note (2) All nine data cards had 0.1 added to Δn.

Note (3) All nine data cards had 0.1 subtracted from Δn.

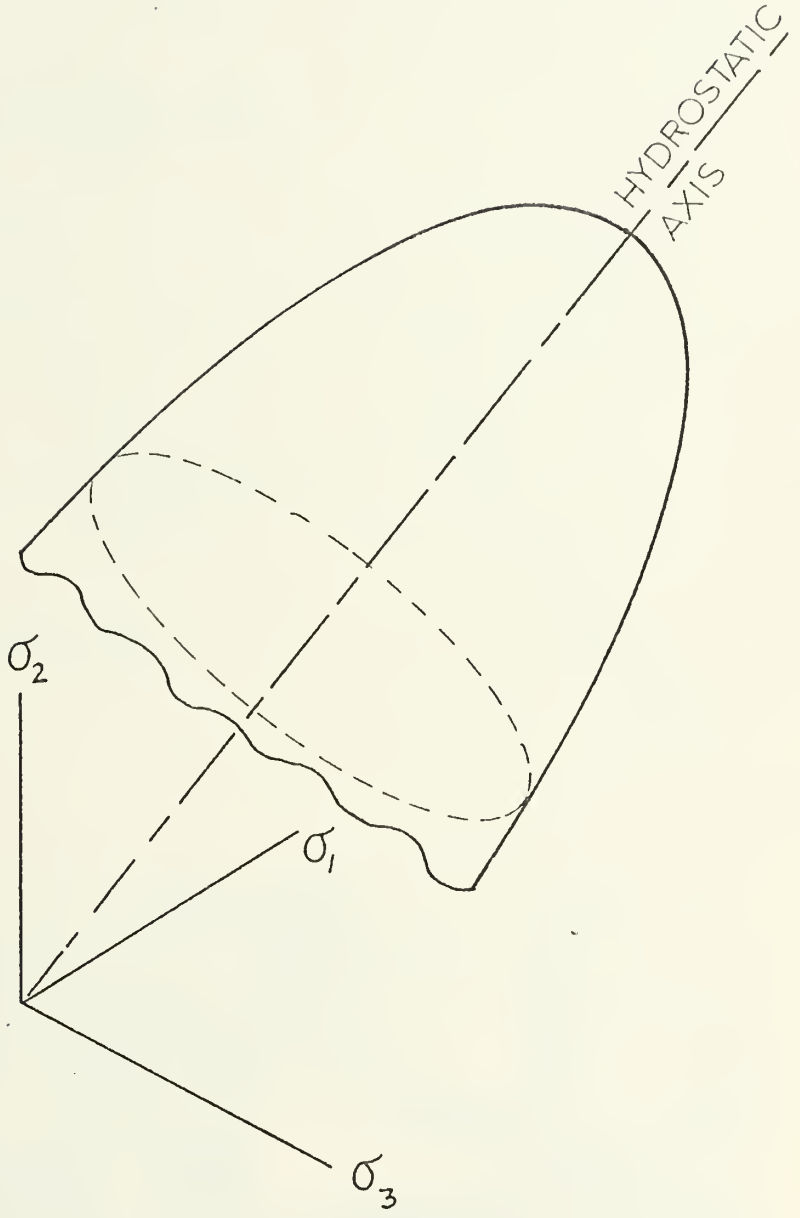

General Shape of Dewetting Criterion Surface in Principle Stress Space

Figure 1

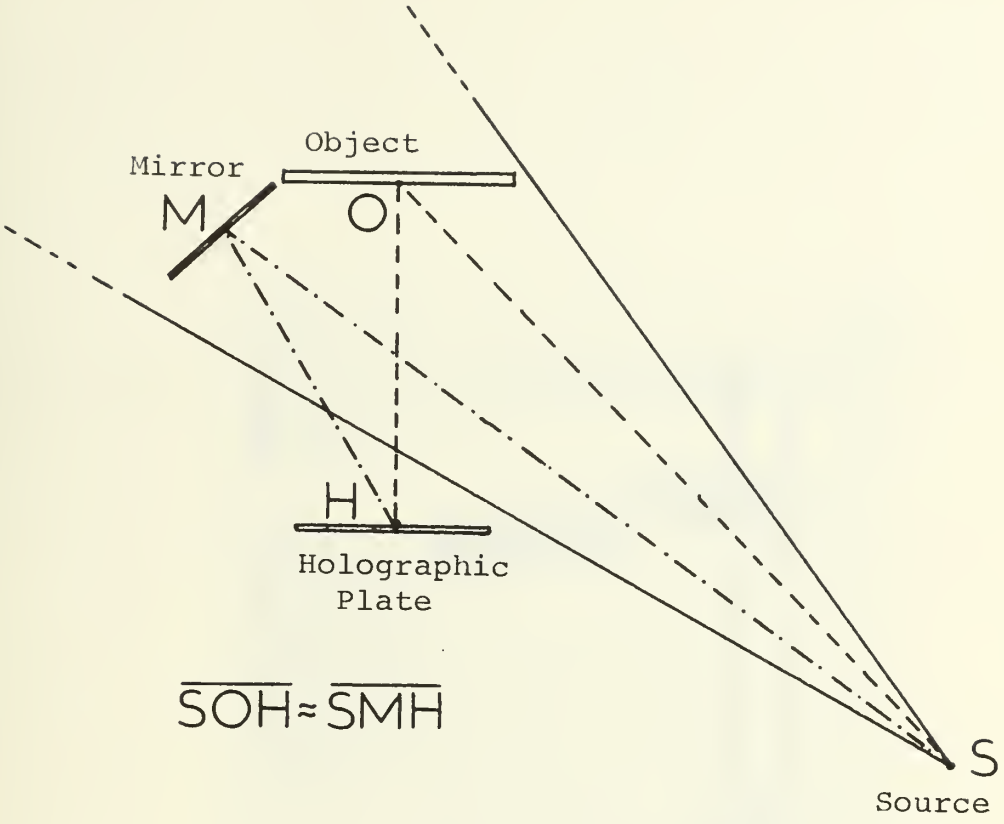

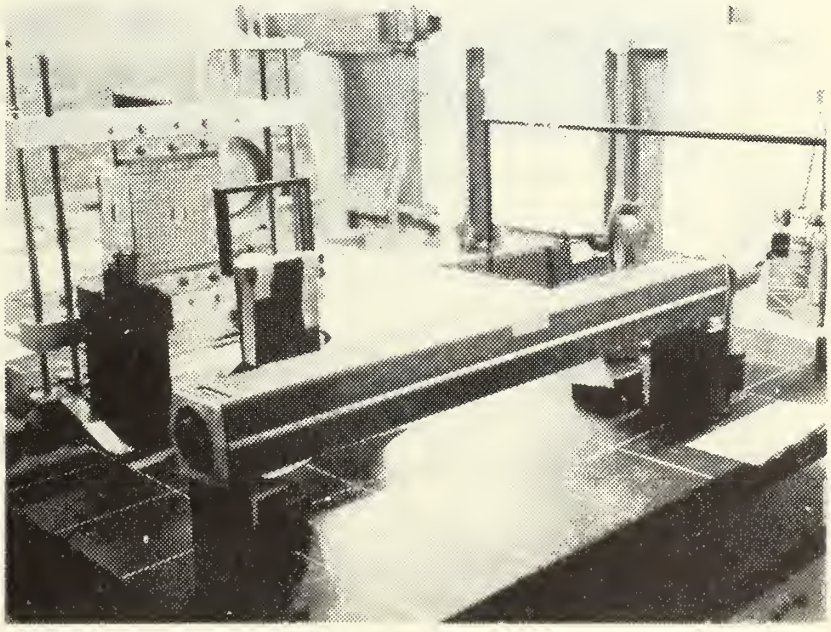

Figure 2 Holographic Setup

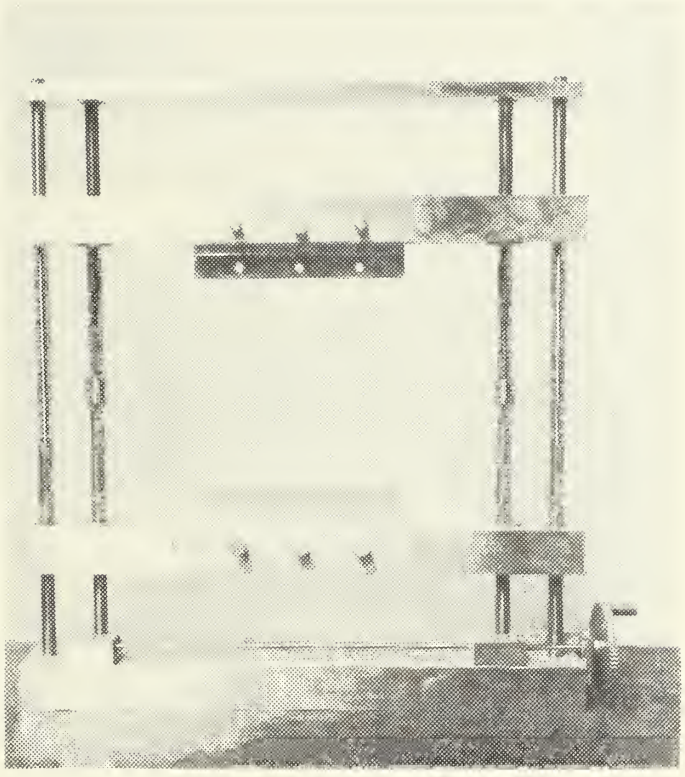

Tensile Testing Machine

Figure 3

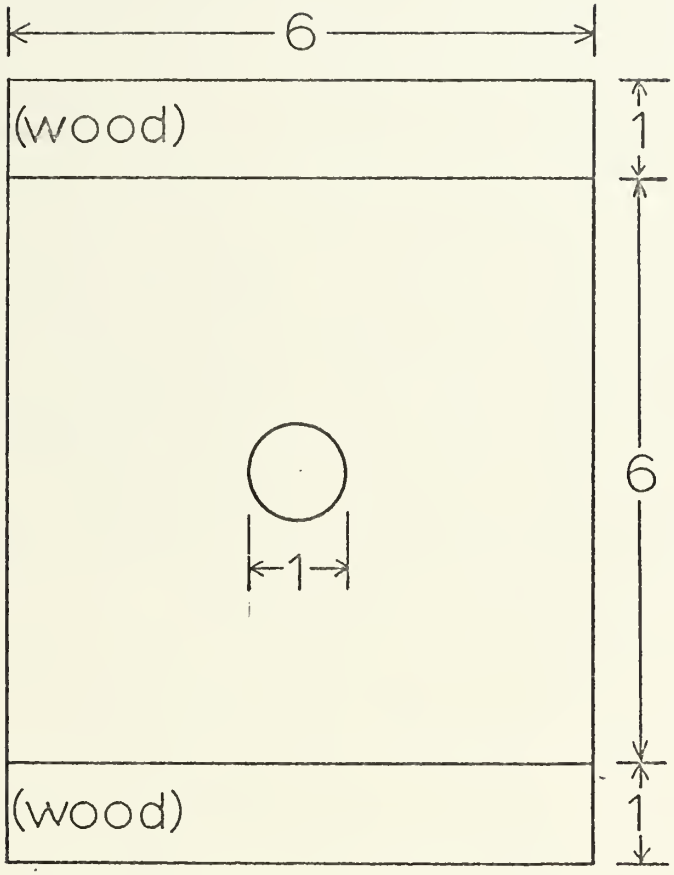

Test Sample Dimensions (in)

Figure 4

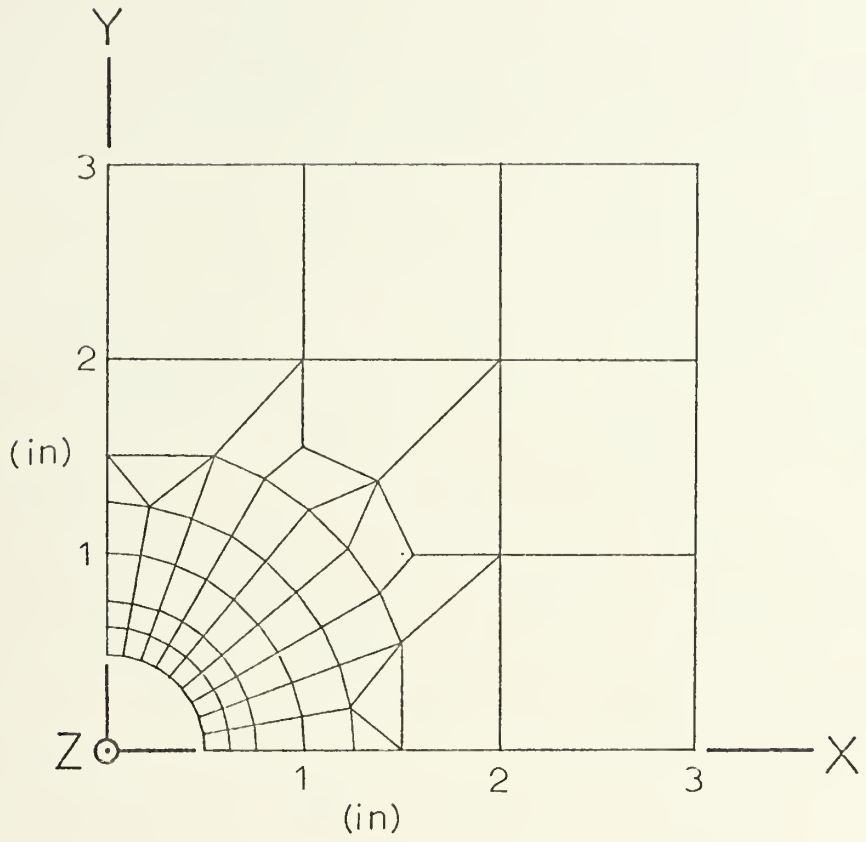

Finite Element Grid

Figure 5

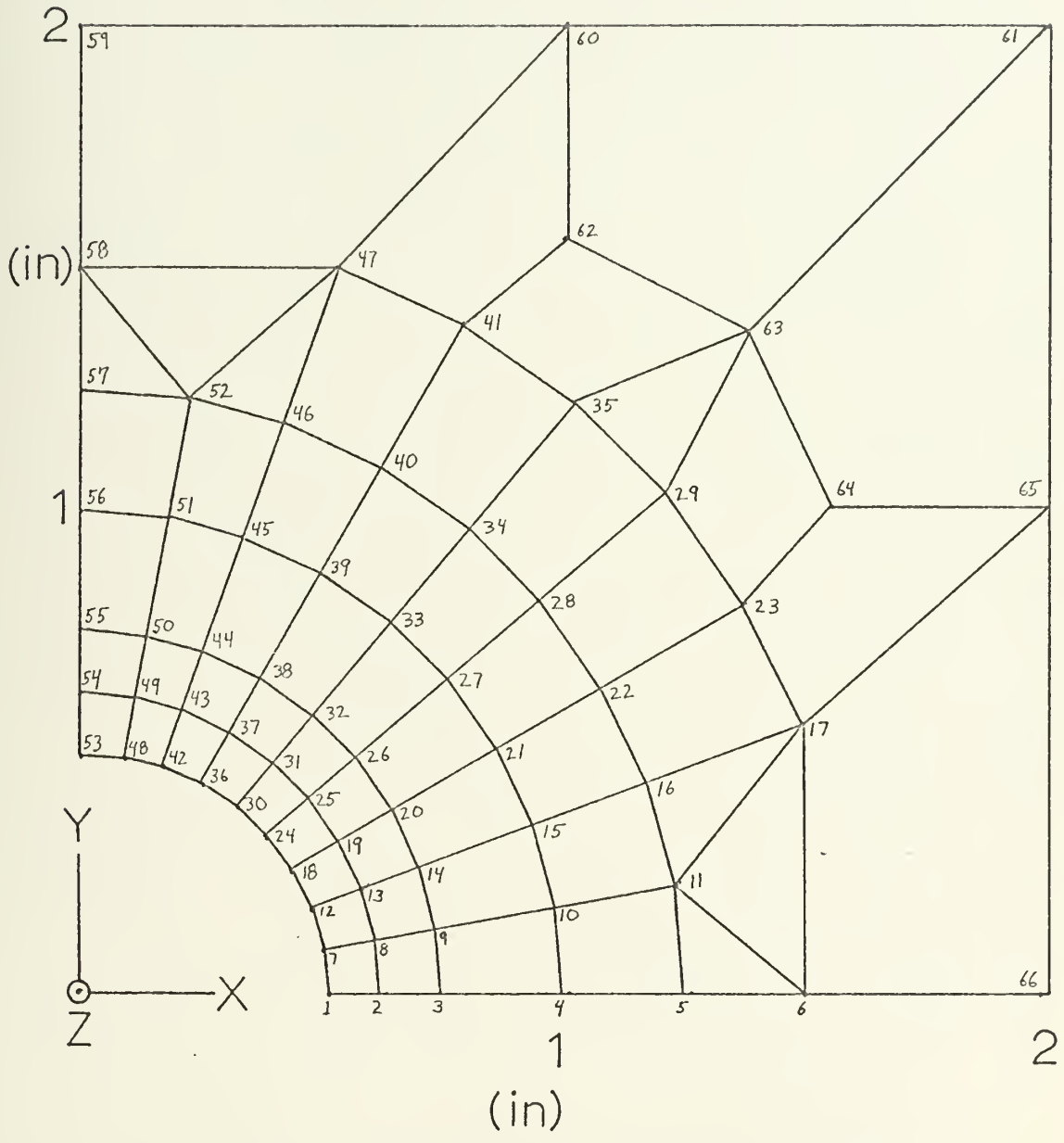

Finite Element Grid with Nodes Numbered

Figure 6

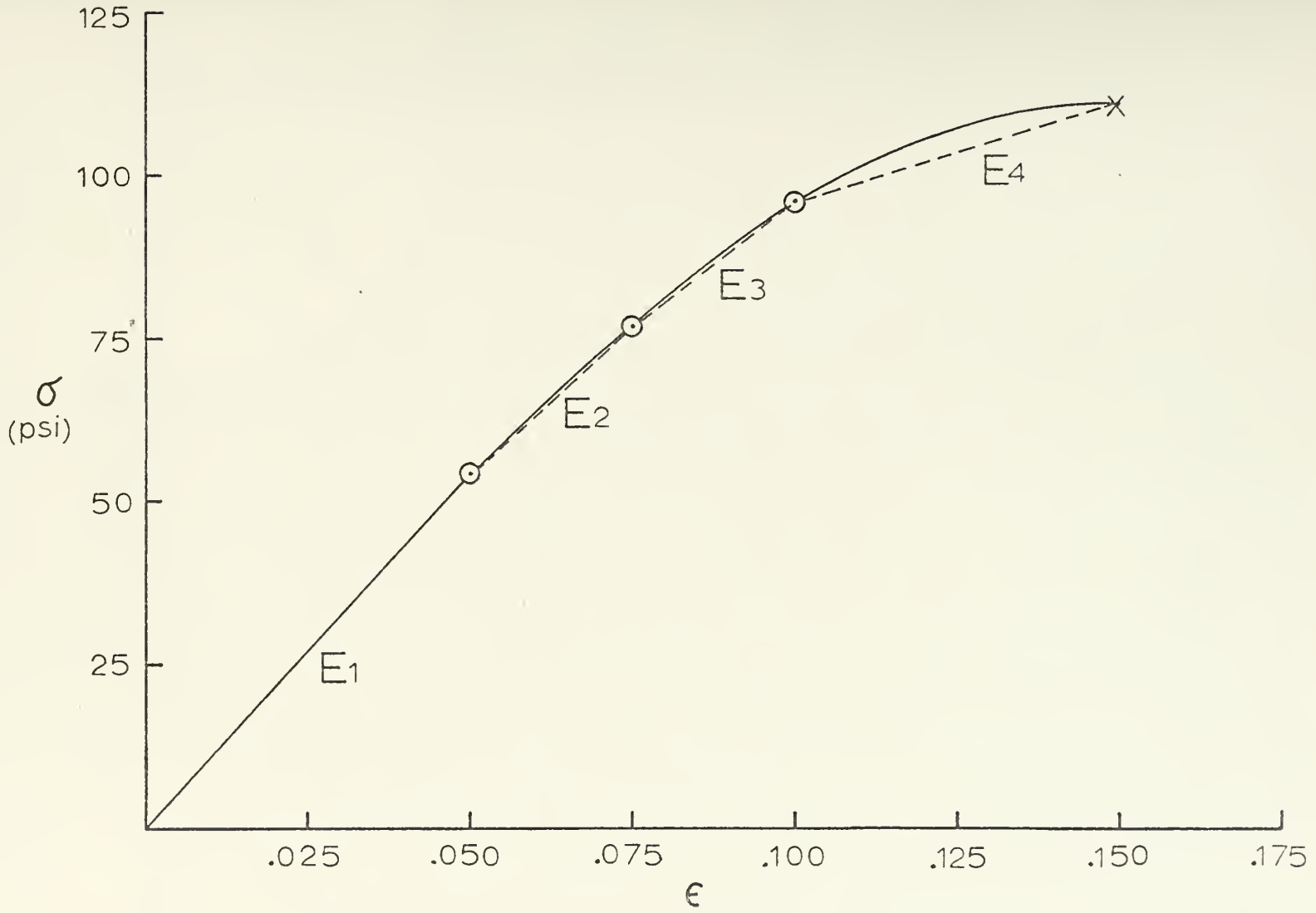

Linearized Stress-Strain Curve for the Filled Sample

Figure 7

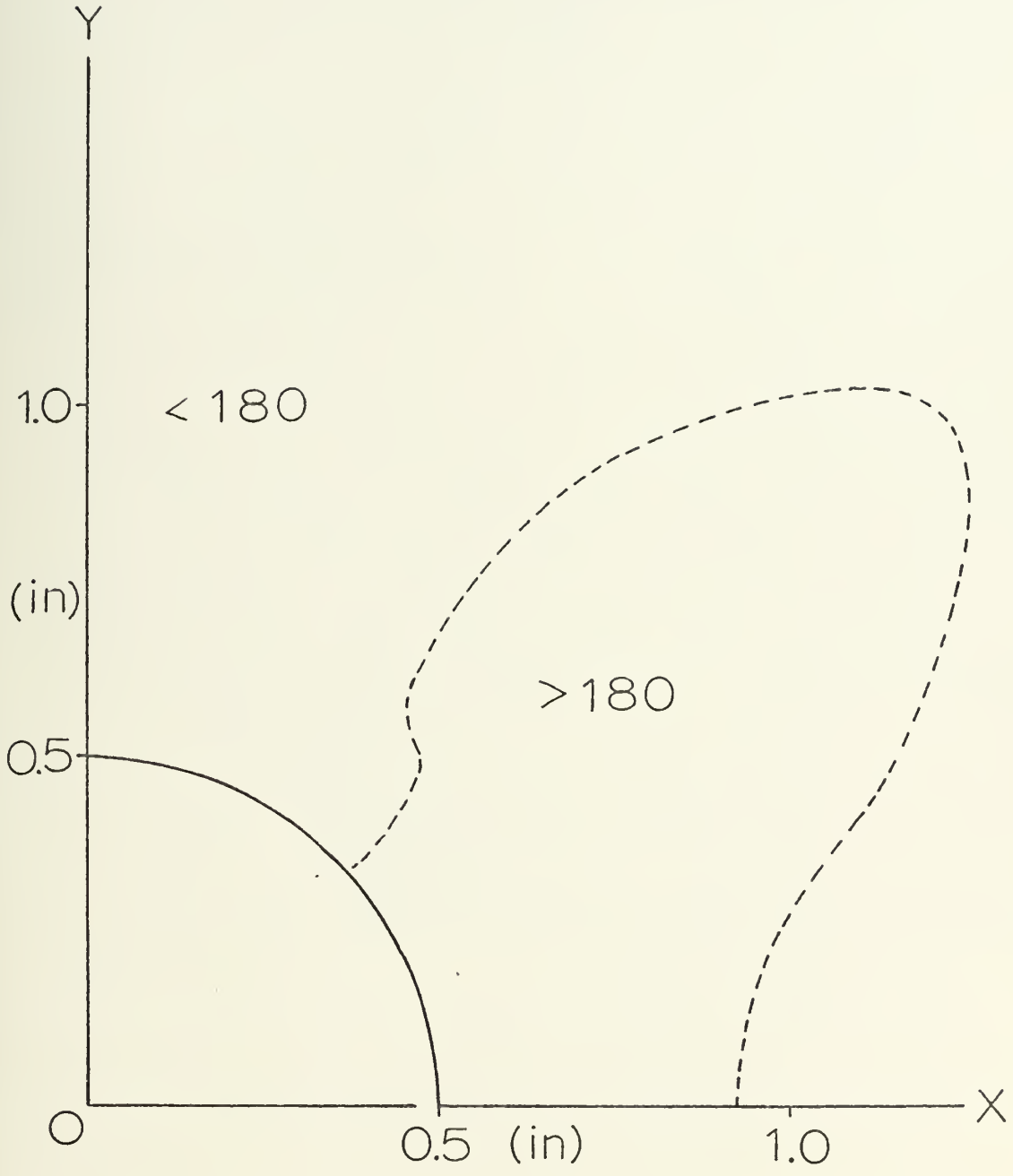

Outline of, $J_2+0.0026(I_1)^2 \geqslant 180$, for an Elastic Material

Figure 8

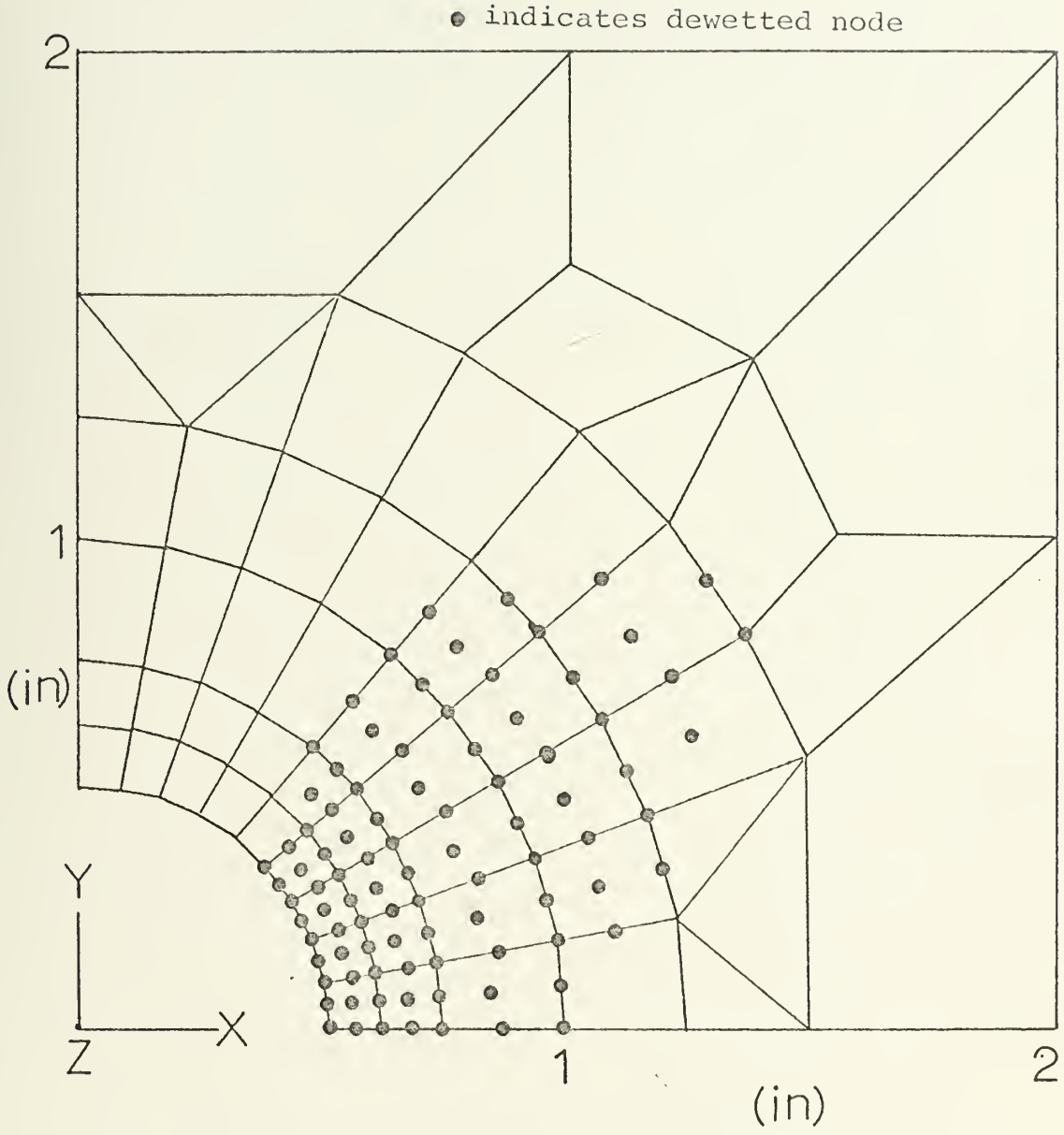

Finite Element Grid Showing Predicted Dewetted Zone in Filled Material at 0.13 Inches Extension

Figure 9

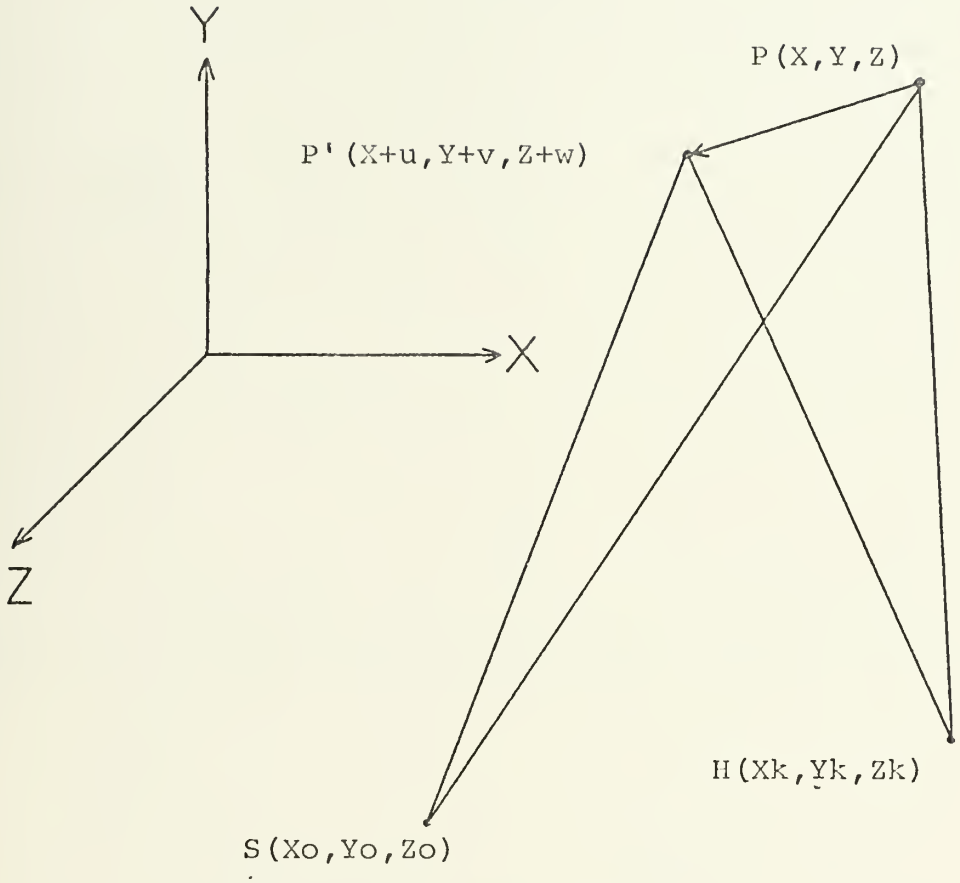

Schematic for Theoretical Analysis

Figure 10

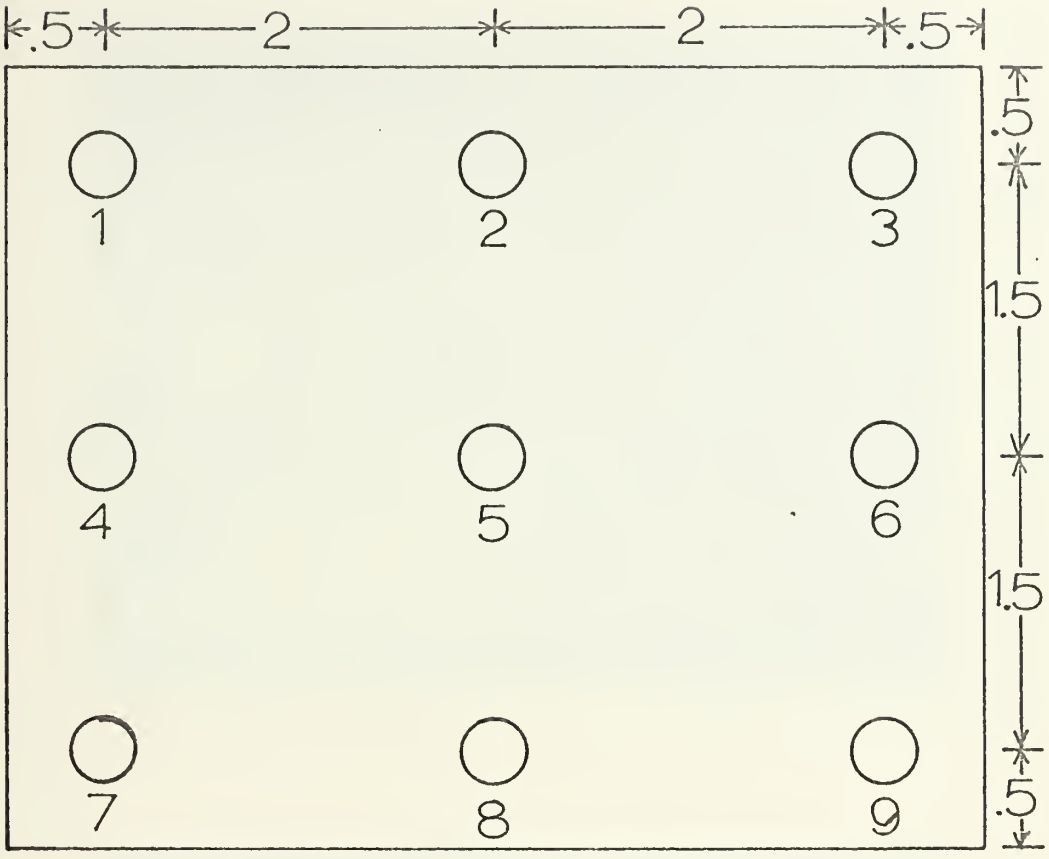

Holographic Plate with Nine Viewports Drawn on the Glass with India Ink

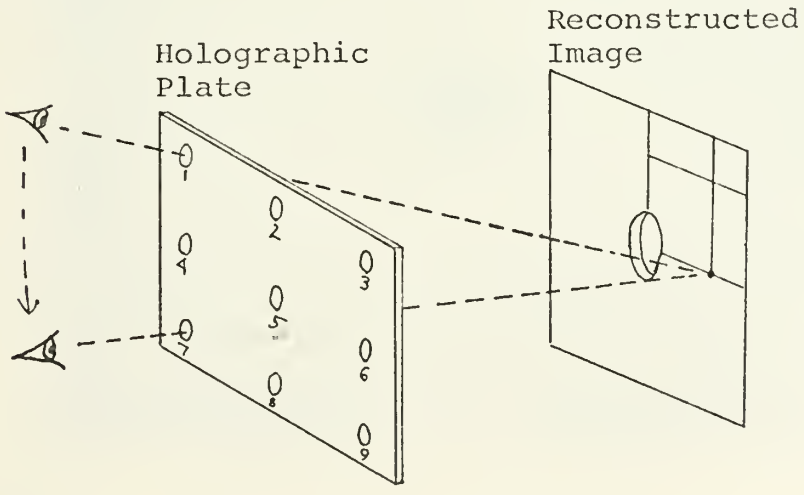

Method of Fringe Counting

Figure 11

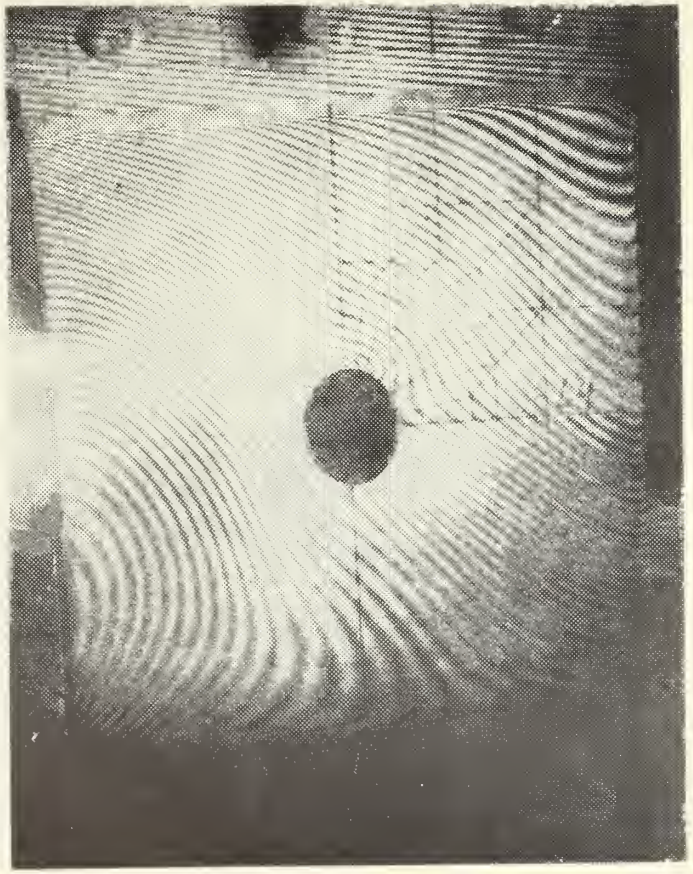

Unfilled Sample used for Fringe Difference Displacement Determination

Figure 12

Filled Sample Used for Fringe Difference Displacement Determination

Figure 13

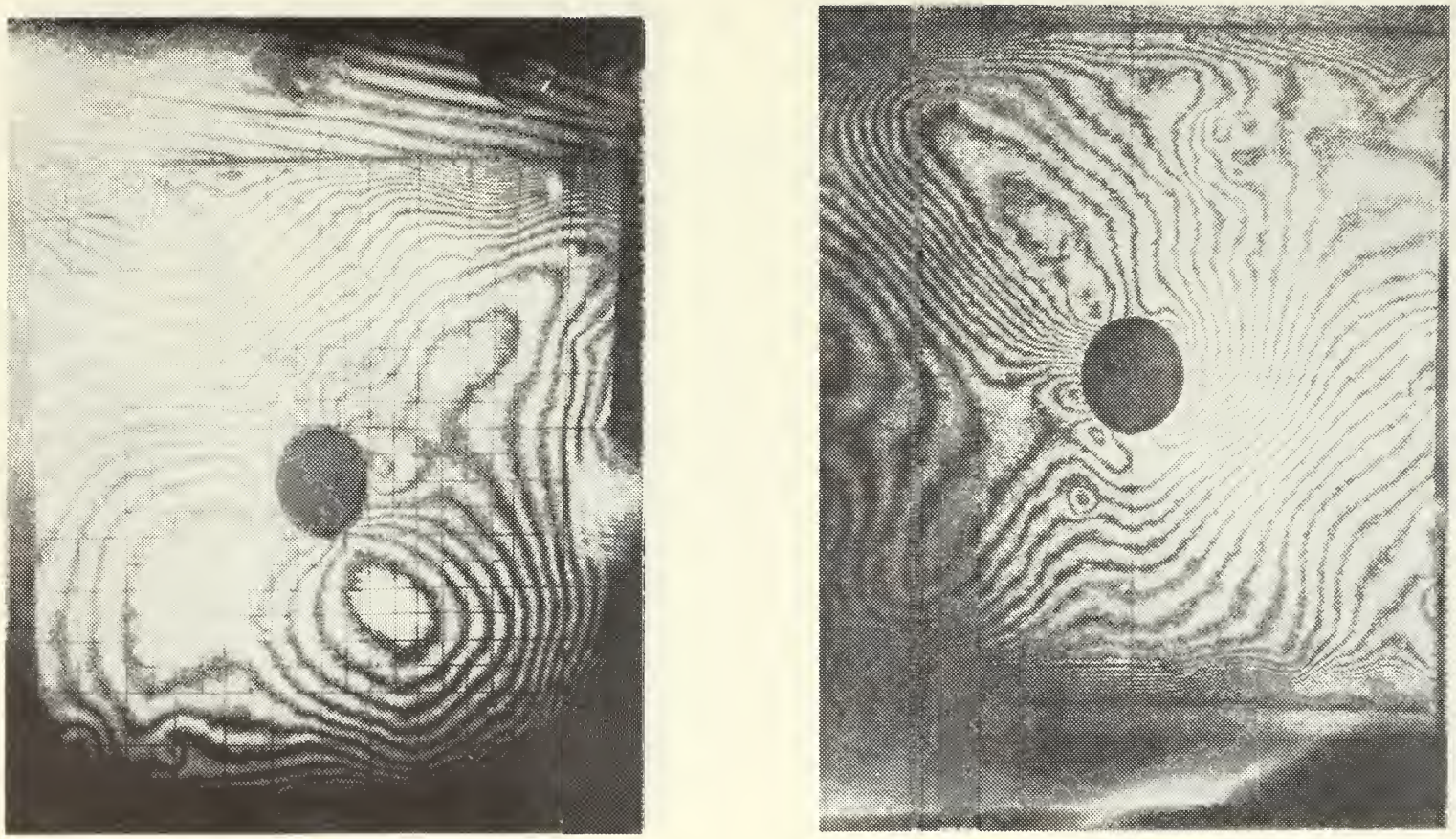

Examples of Residual Strain Interferograms

Figure 14

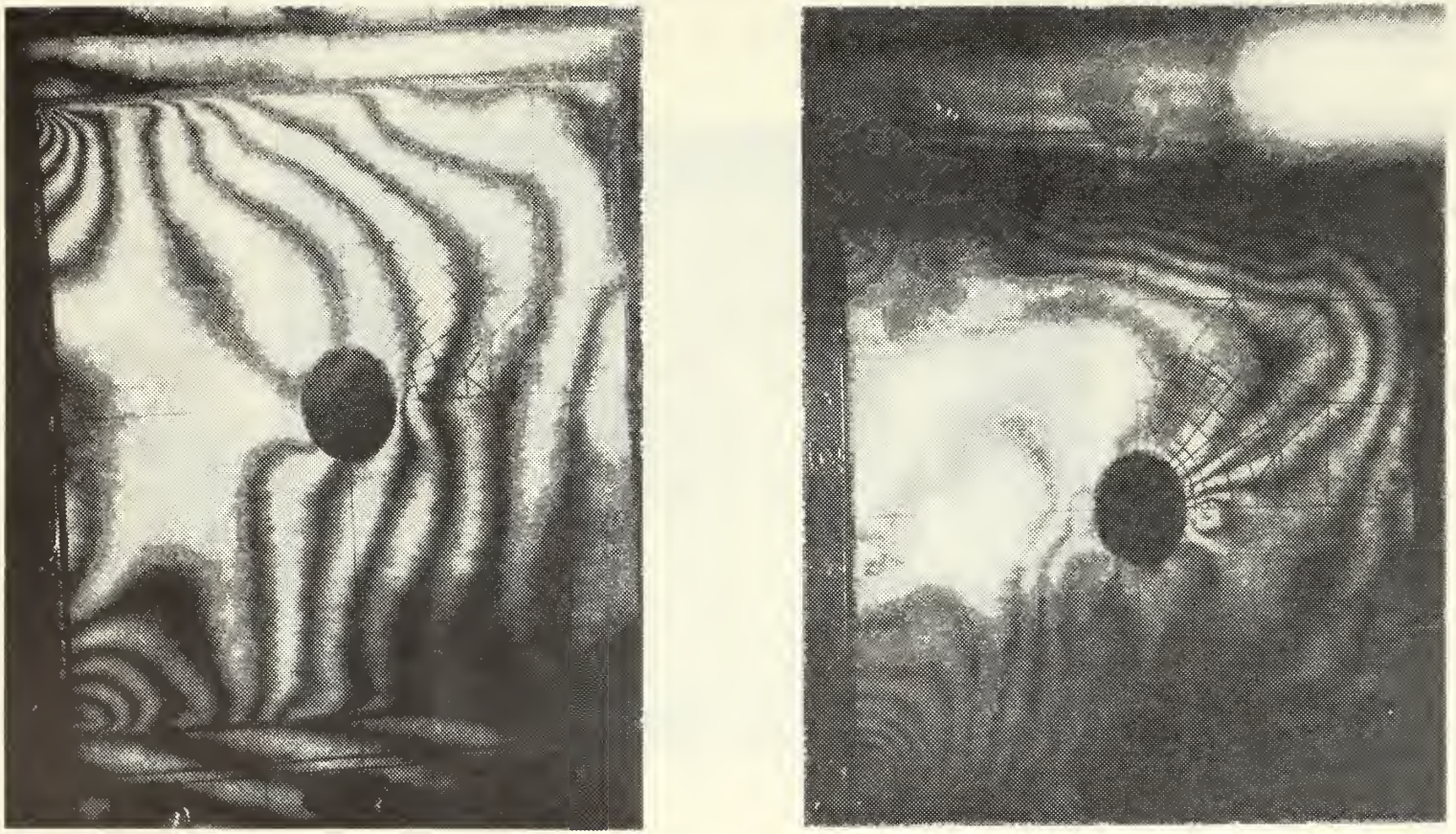

Example of Residual Strain Interferograms

Figure 15

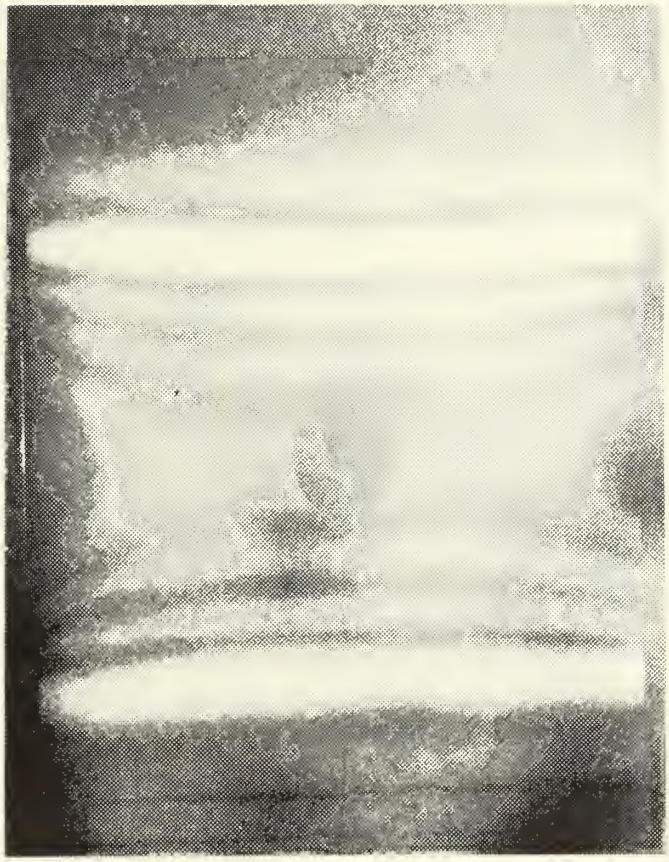

Time Average Hologram of Filled Sample Excited at 120 CPS

Figure 16

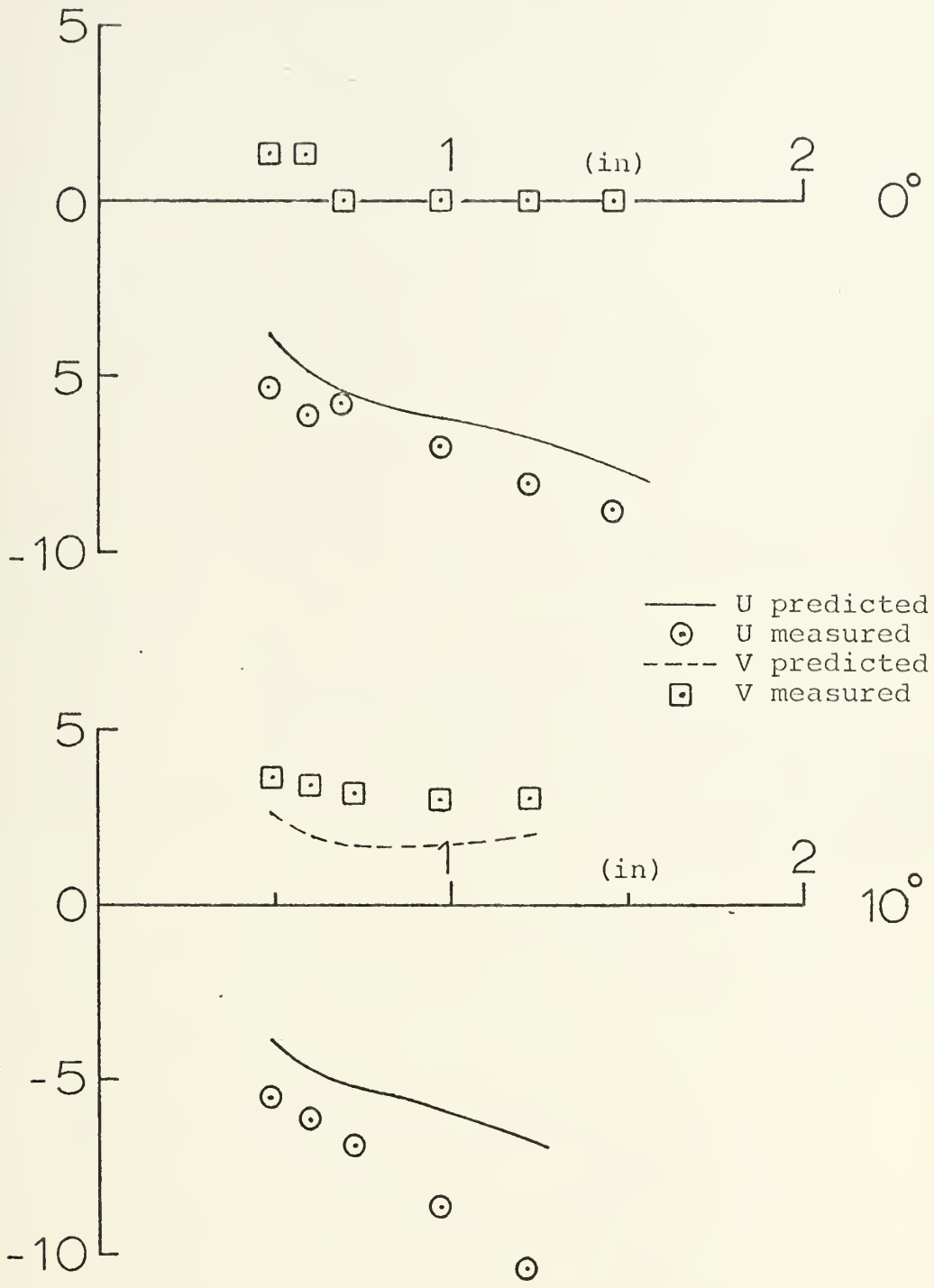

Unfilled Nondimensional Displacements vs Radial Distance

Figure 17

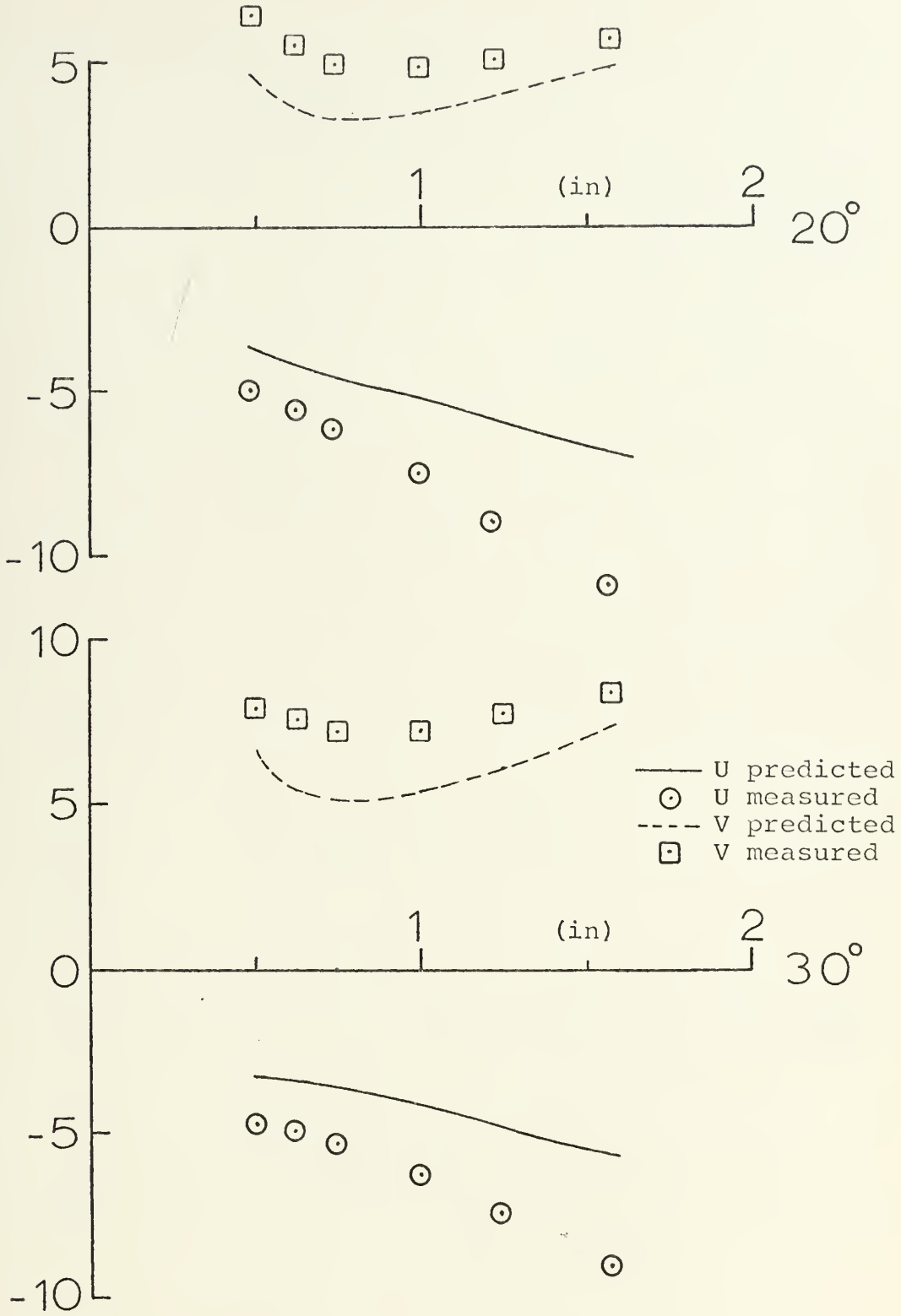

Unfilled Nondimensional Displacements vs Radial Distance

Figure 18

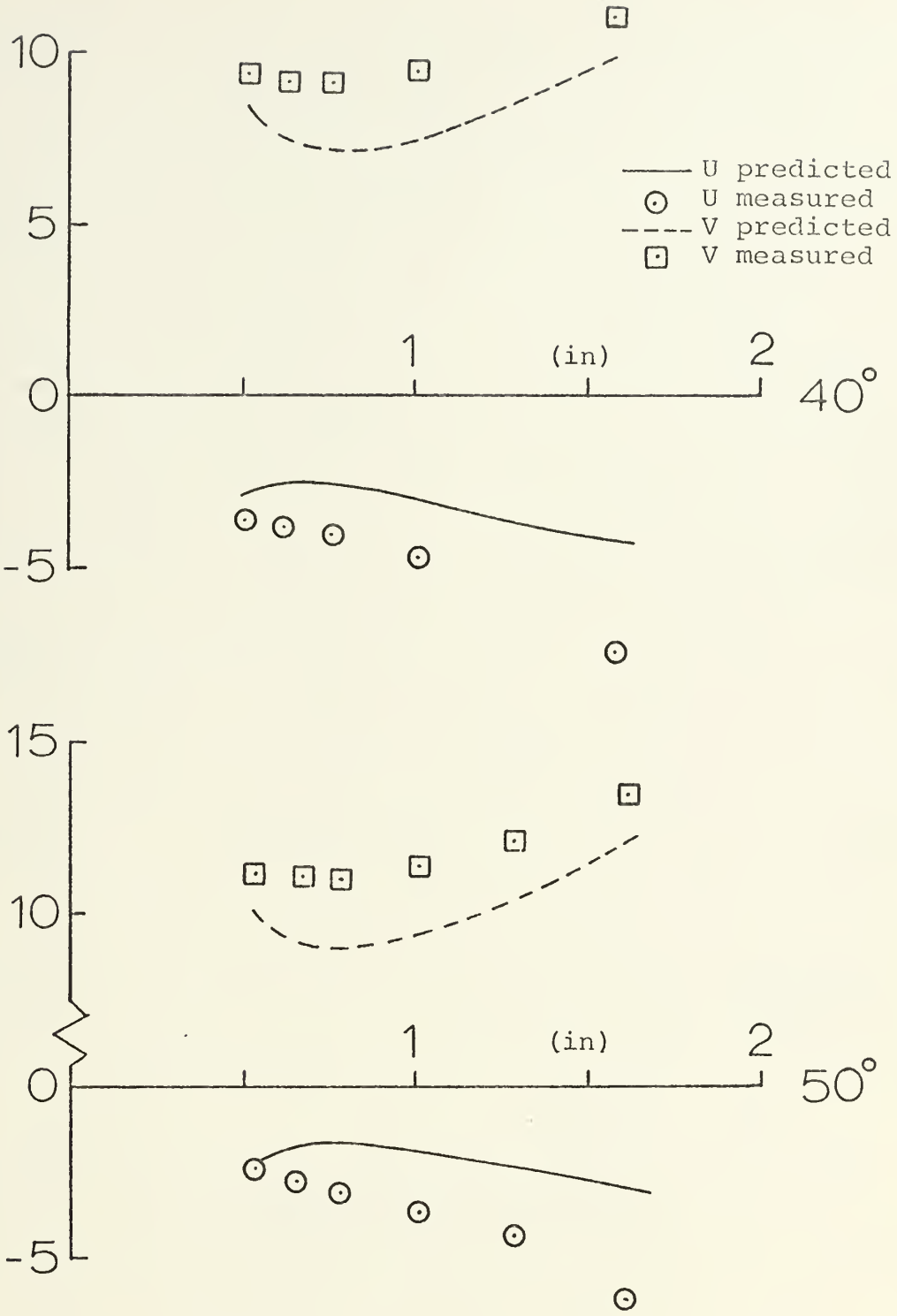

Unfilled Nondimensional Displacements vs Radial Distance

Figure 19

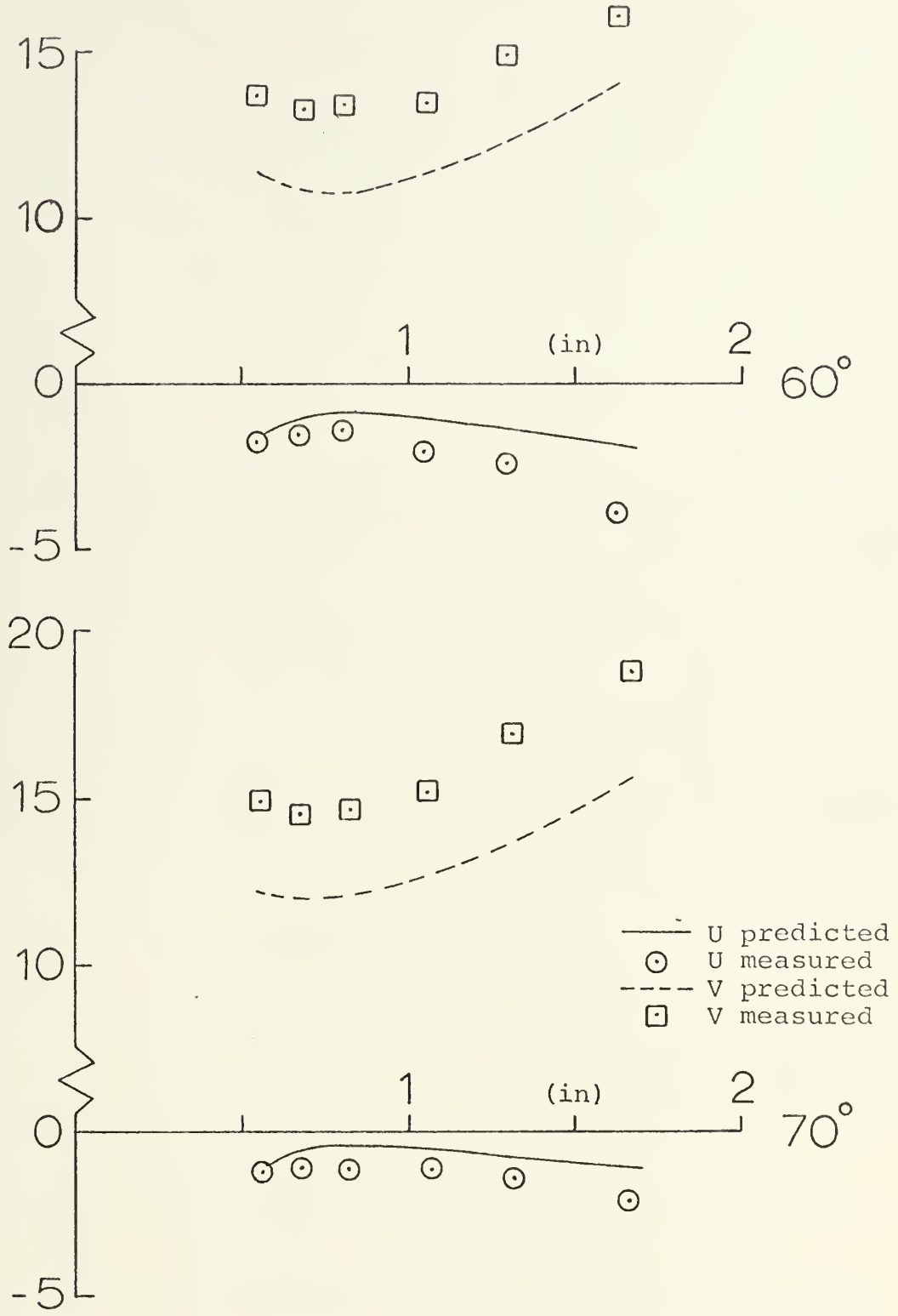

Unfilled Nondimensional Displacements vs Radial Distance

Figure 20

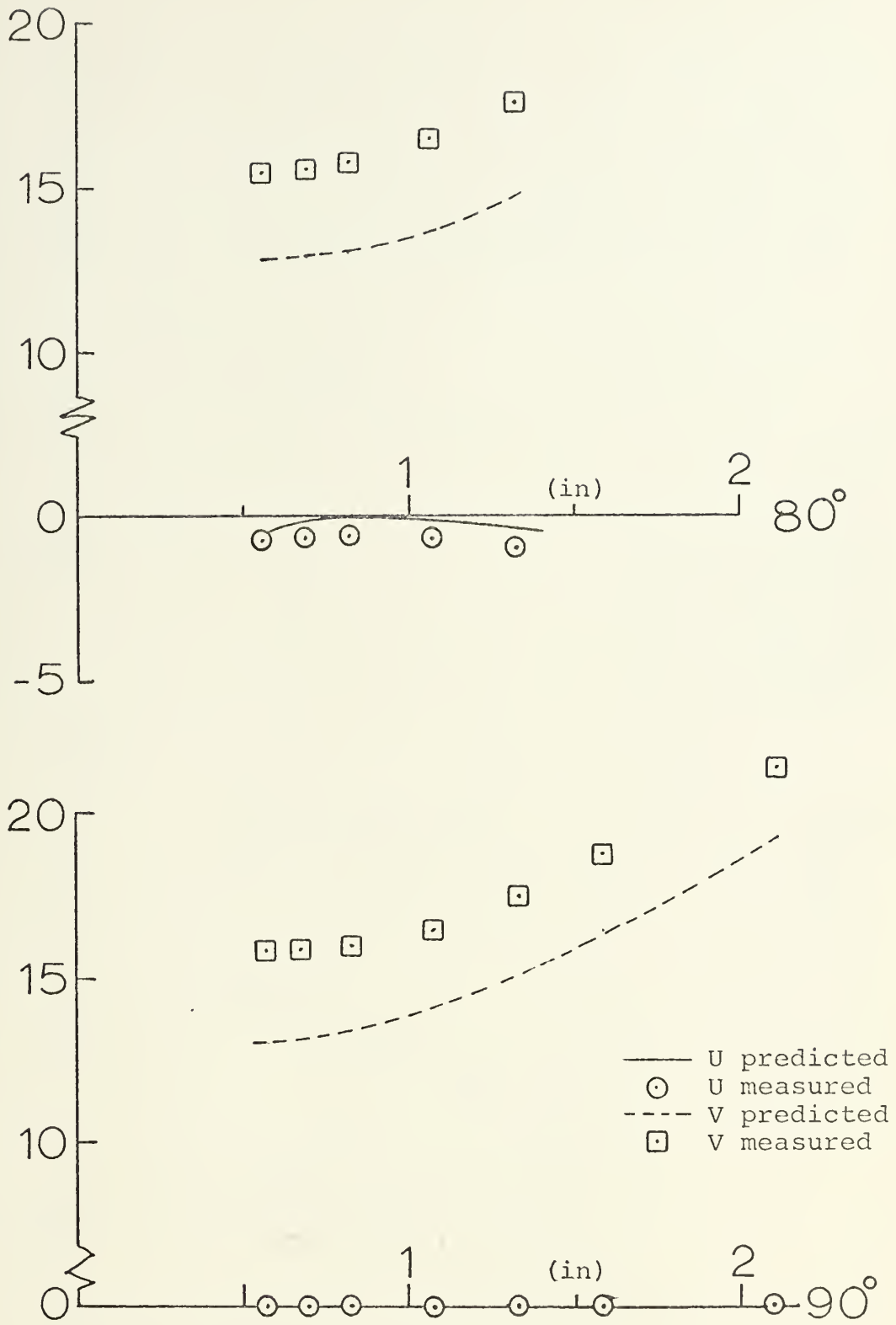

Unfilled Nondimensional Displacements vs Radial Distance

Figure 21

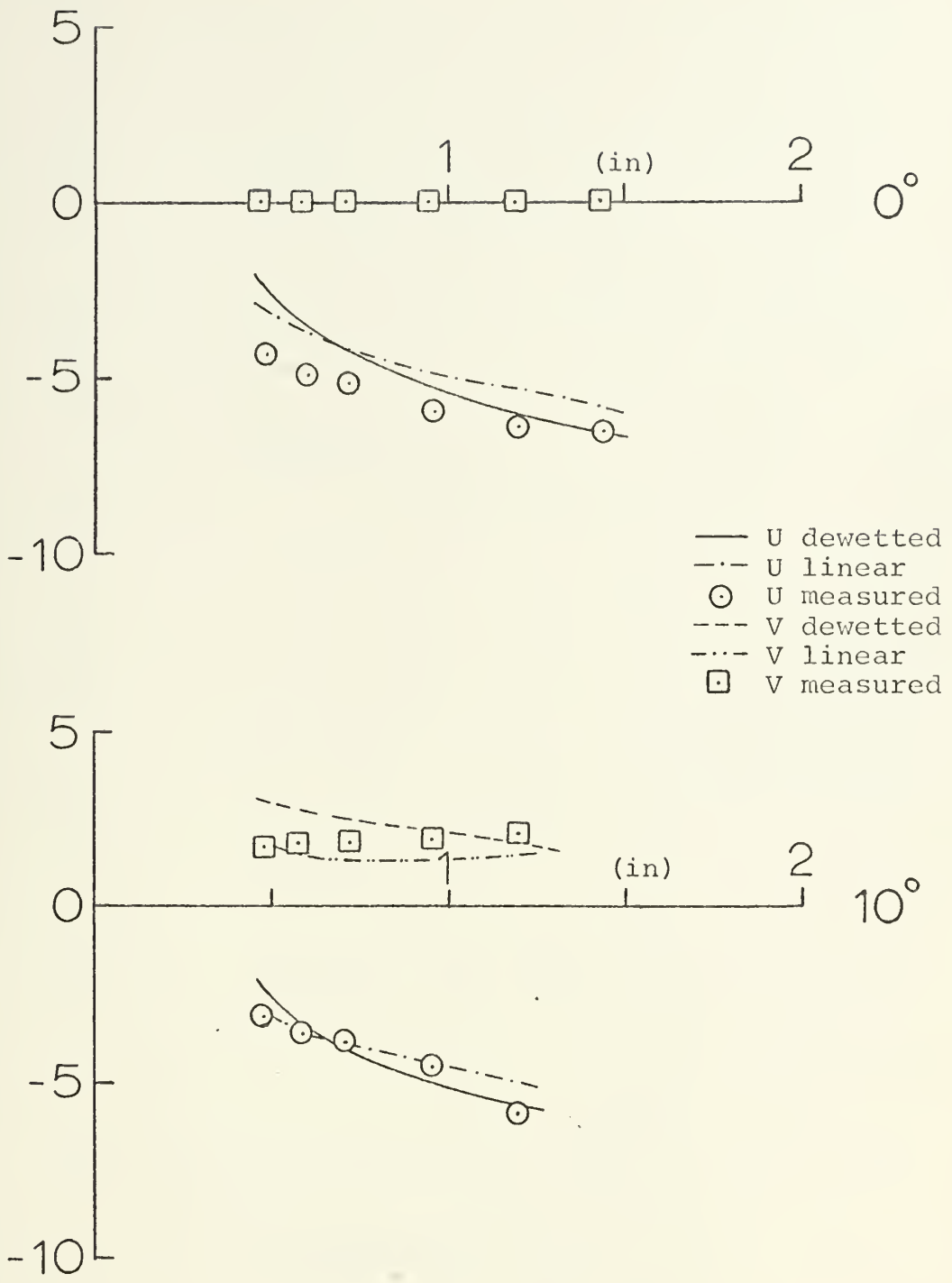

Filled Nondimensional Displacements vs Radial Distance

Figure 22

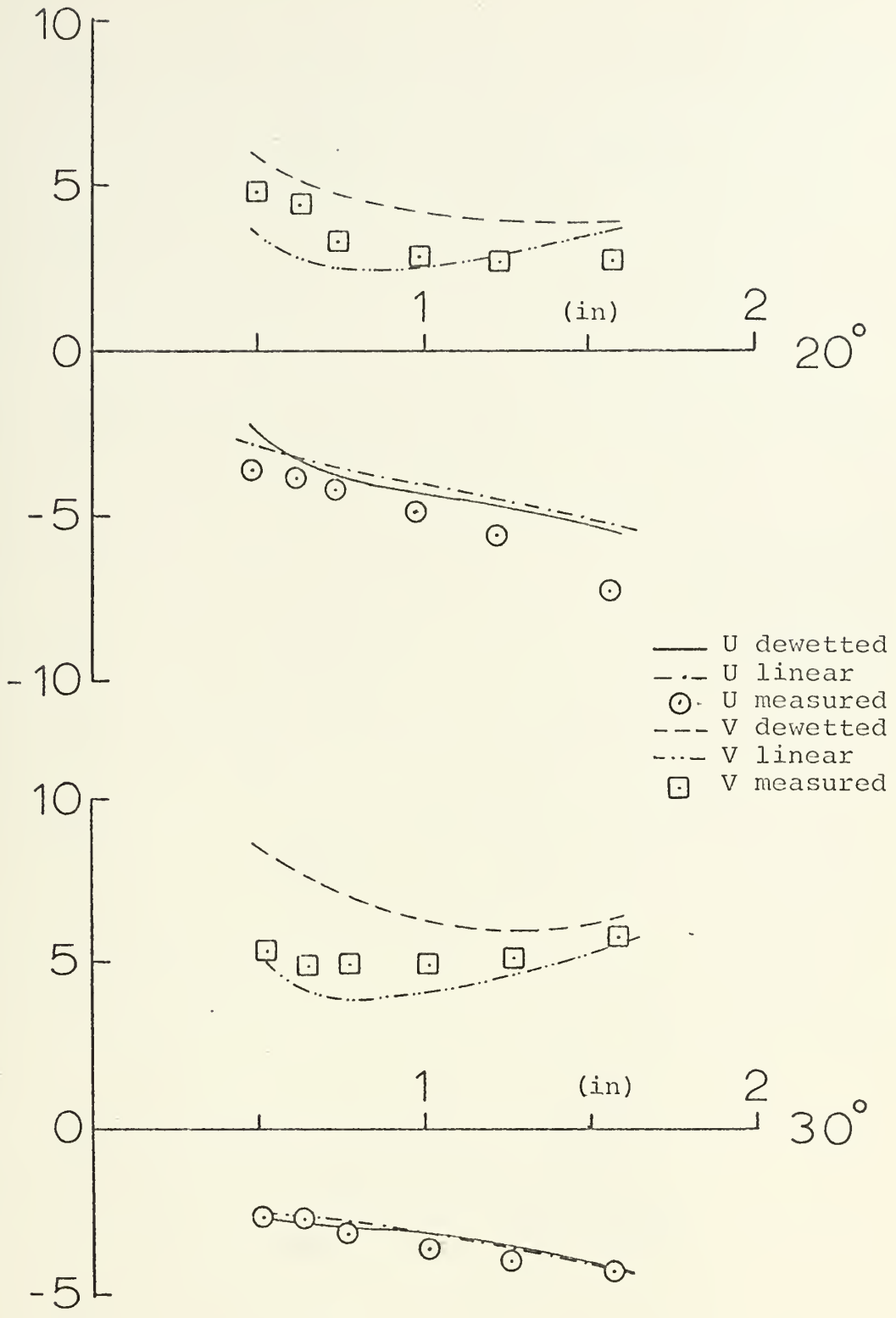

Filled Nondimensional Displacements vs Radial Distance

Figure 23

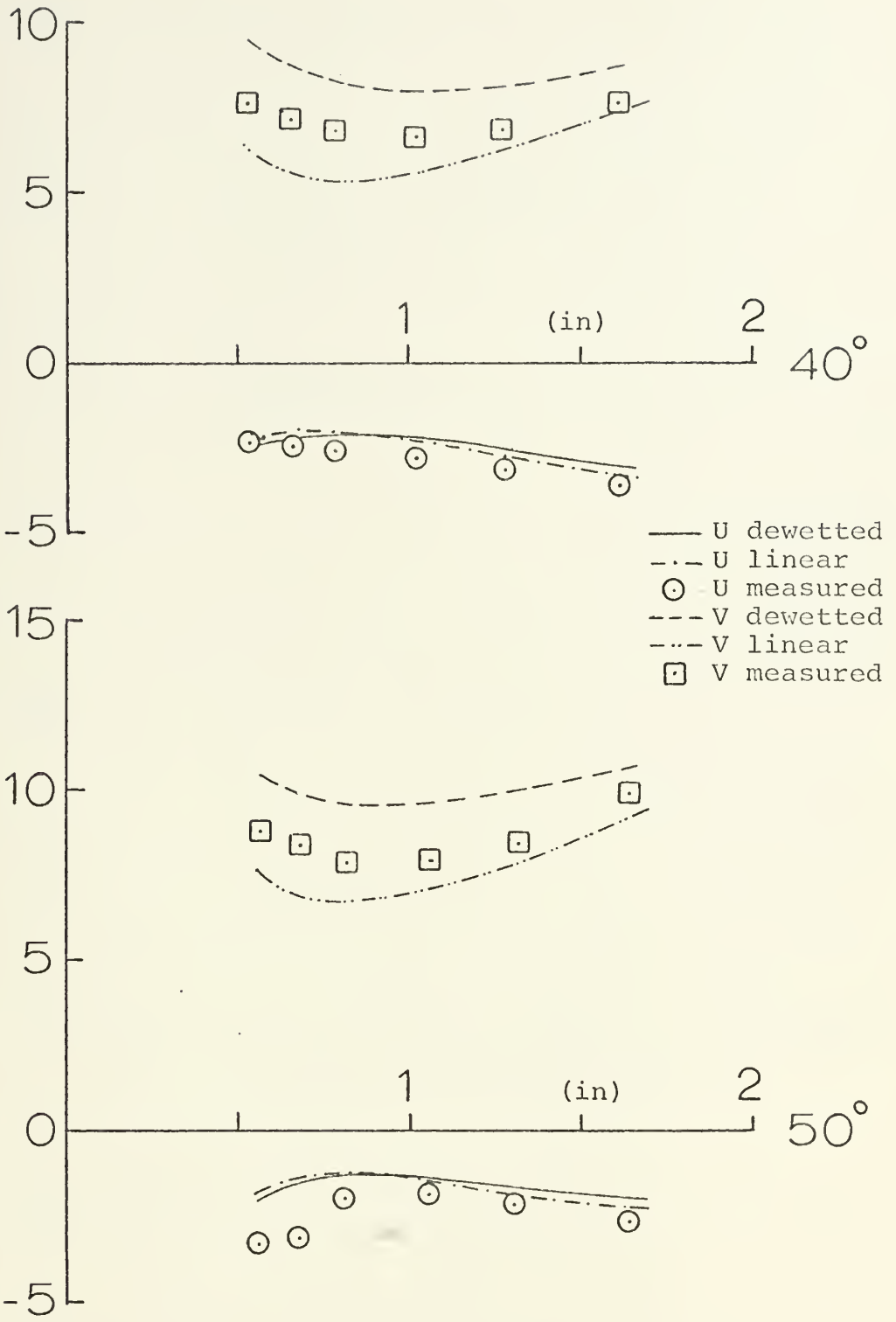

Filled Nondimensional Displacements vs Radial Distance

Figure 24

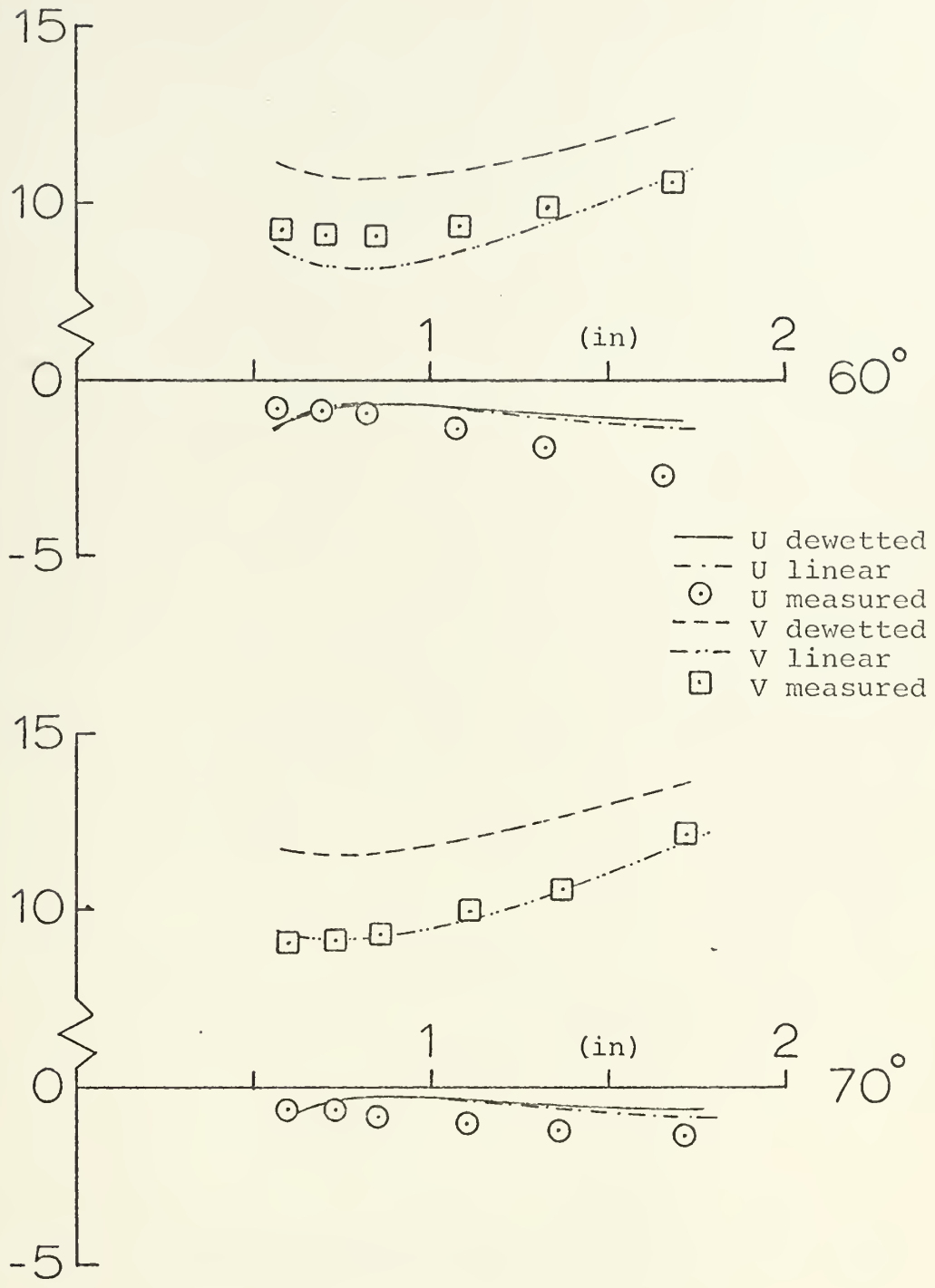

Filled Nondimensional Displacements vs Radial Distance

Figure 25

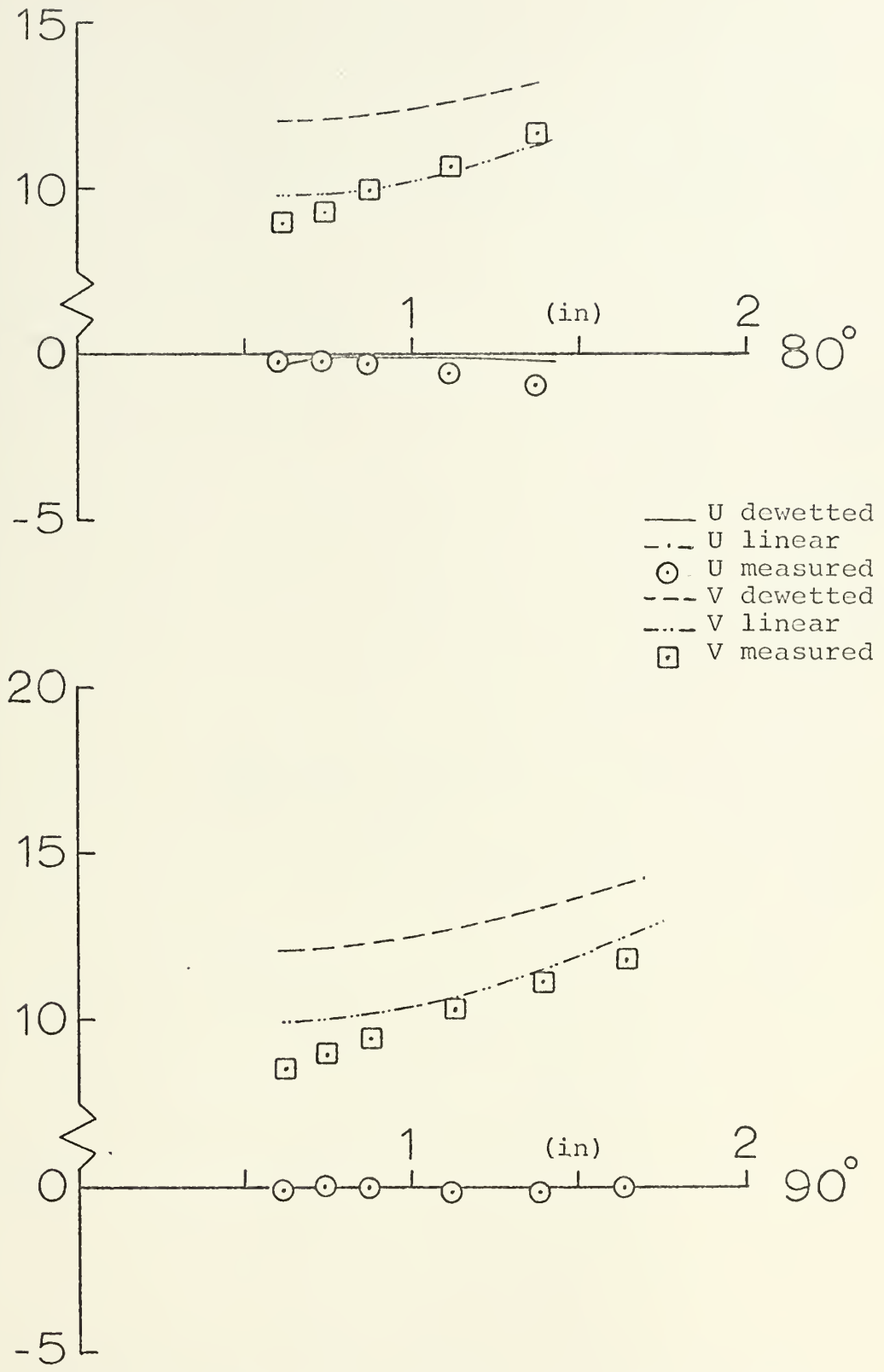

Filled Nondimensional Displacements vs Radial Distance

Figure 26

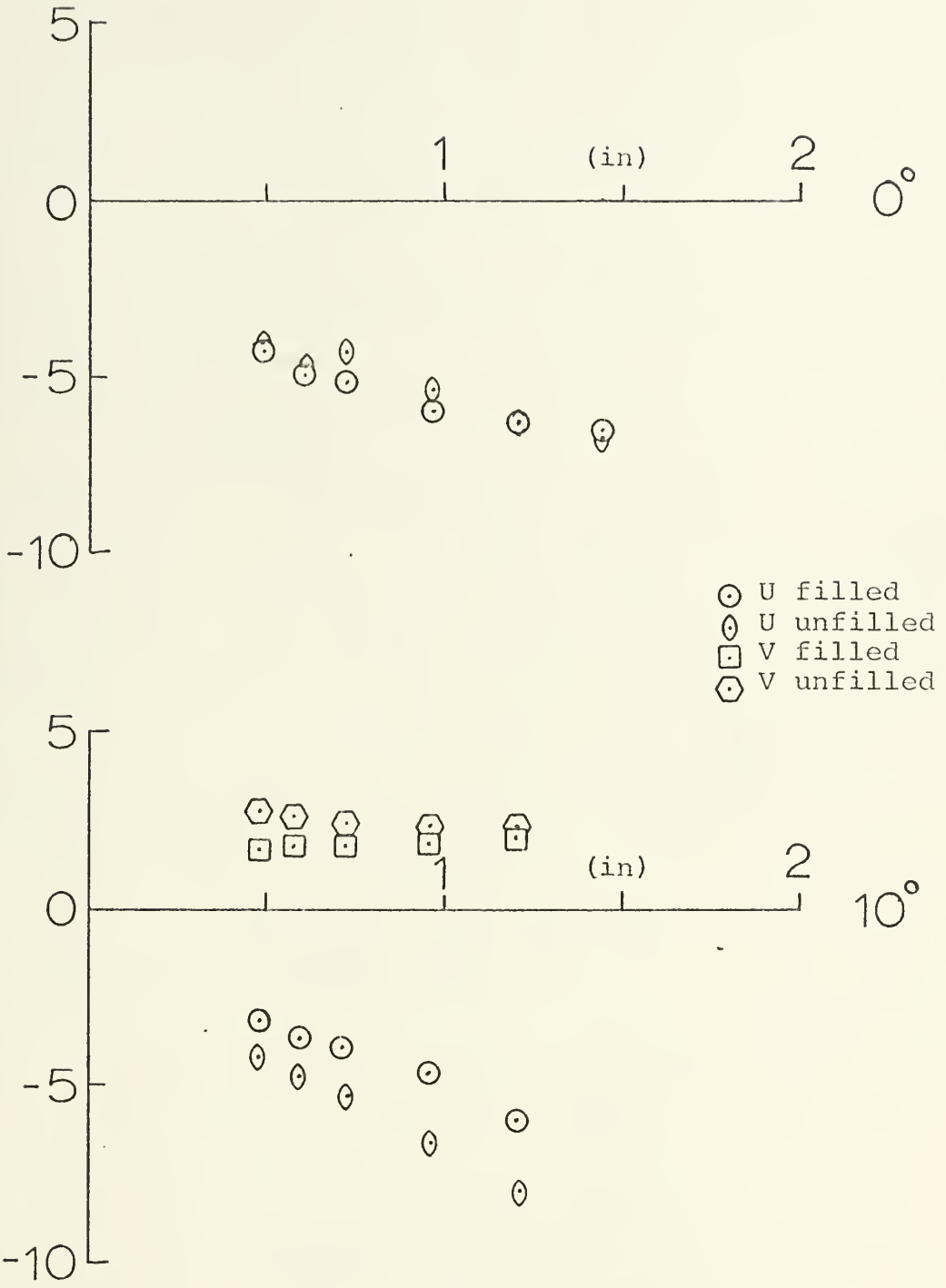

Nondimensional Displacements vs Radial Distance

Figure 27

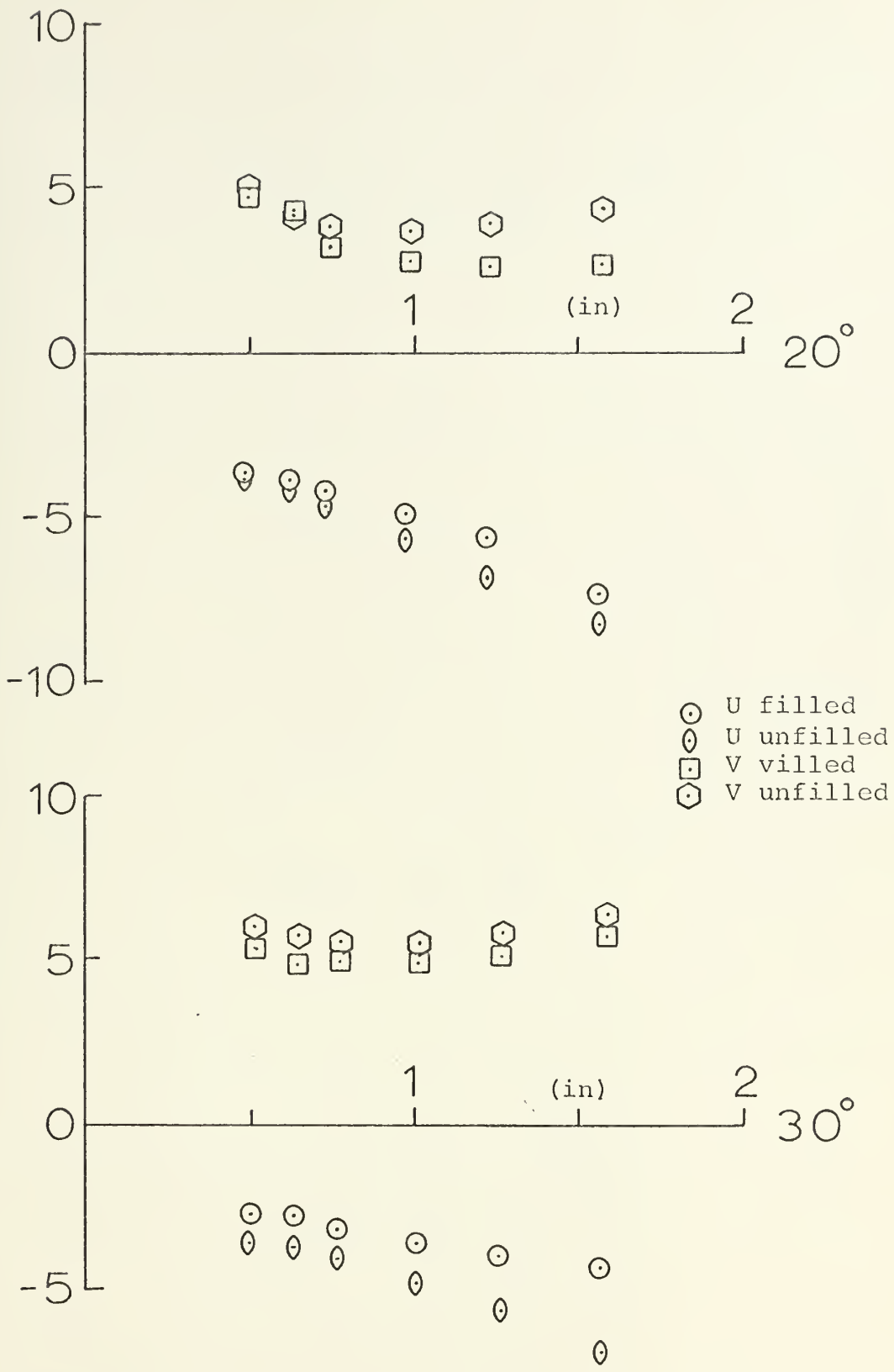

Nondimensional Displacements vs Radial Distance

Figure 28

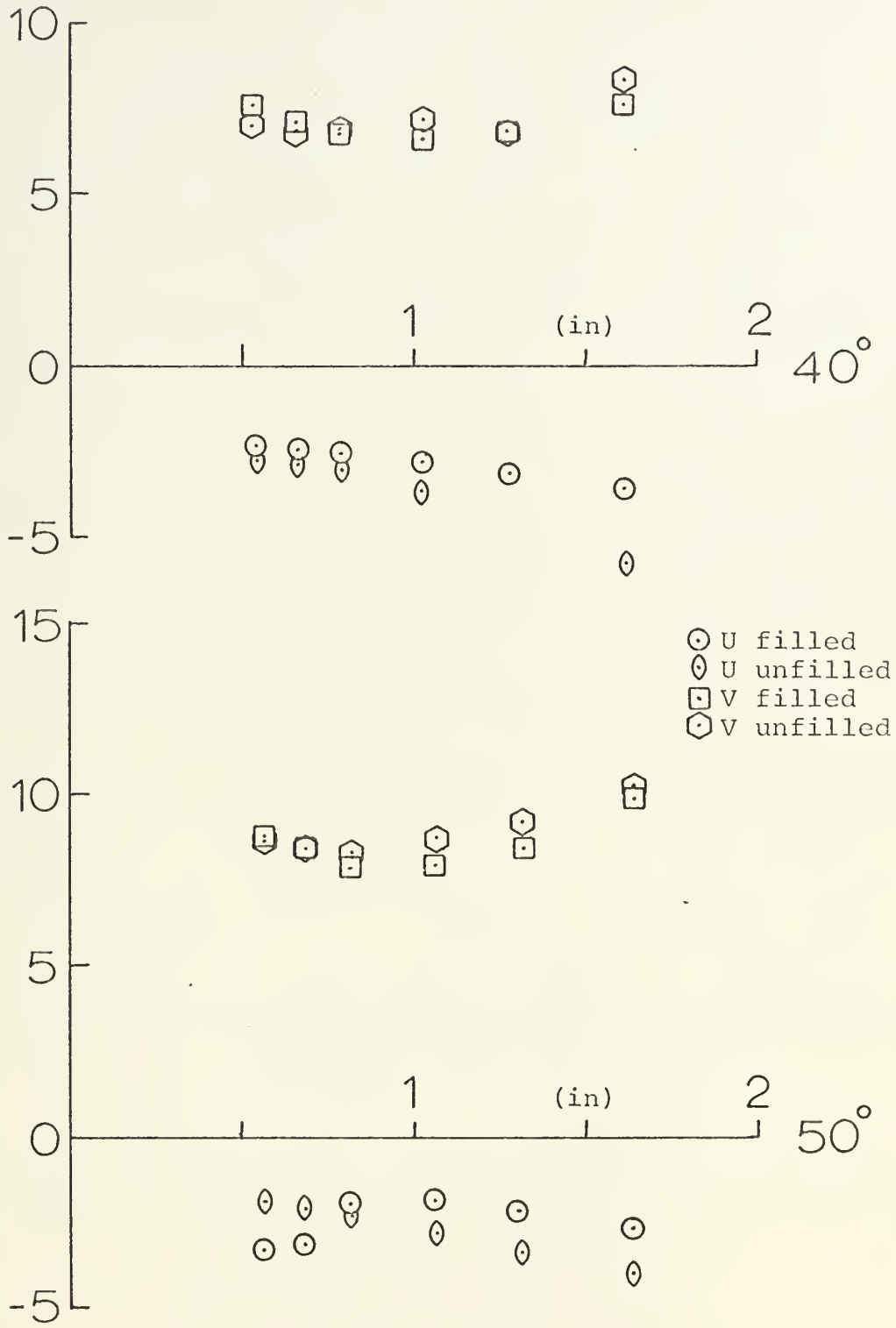

Nondimensional Displacements vs Radial Distance

Figure 29

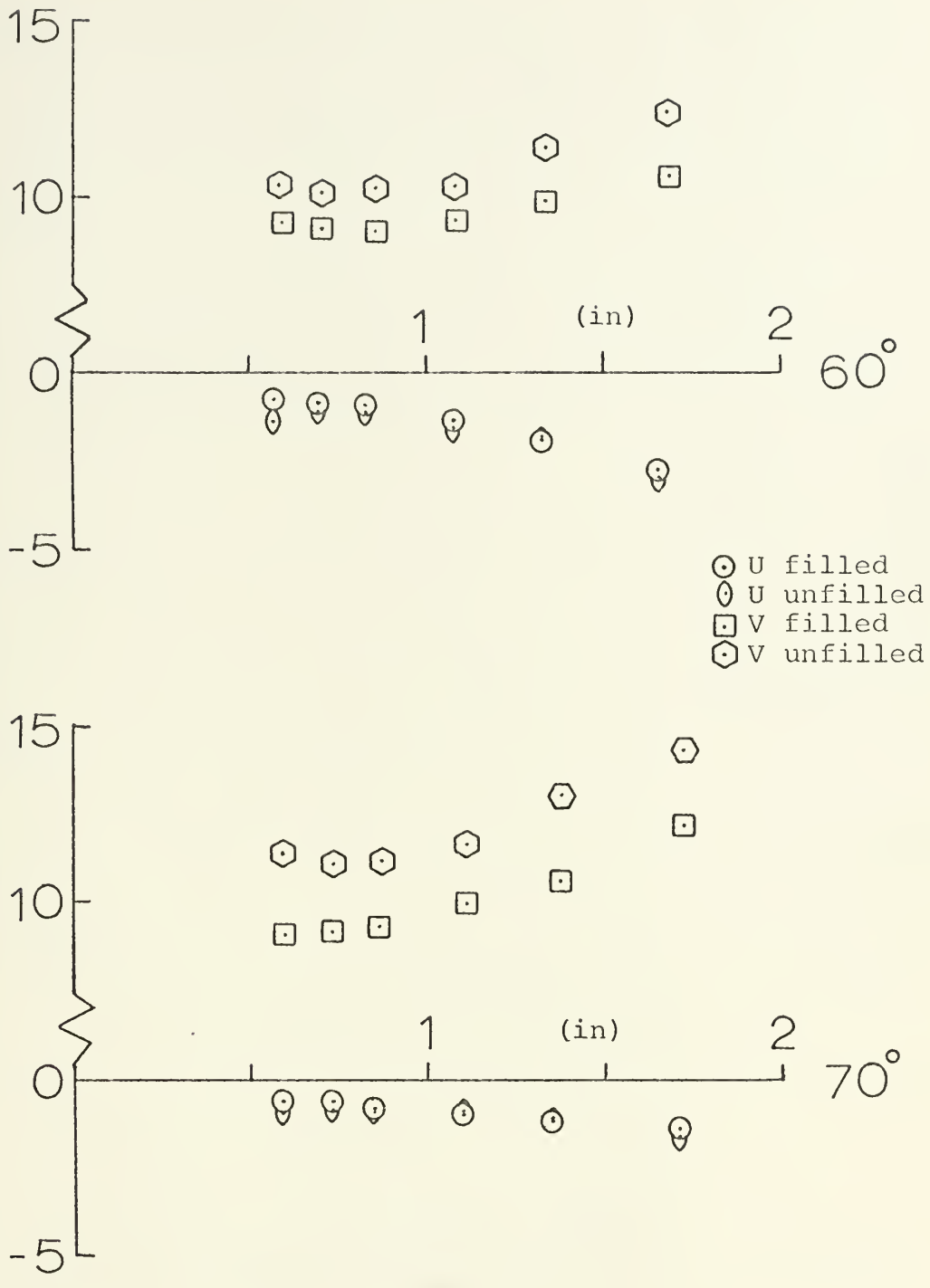

Nondimensional Displacements vs Radial Distance

Figure 30

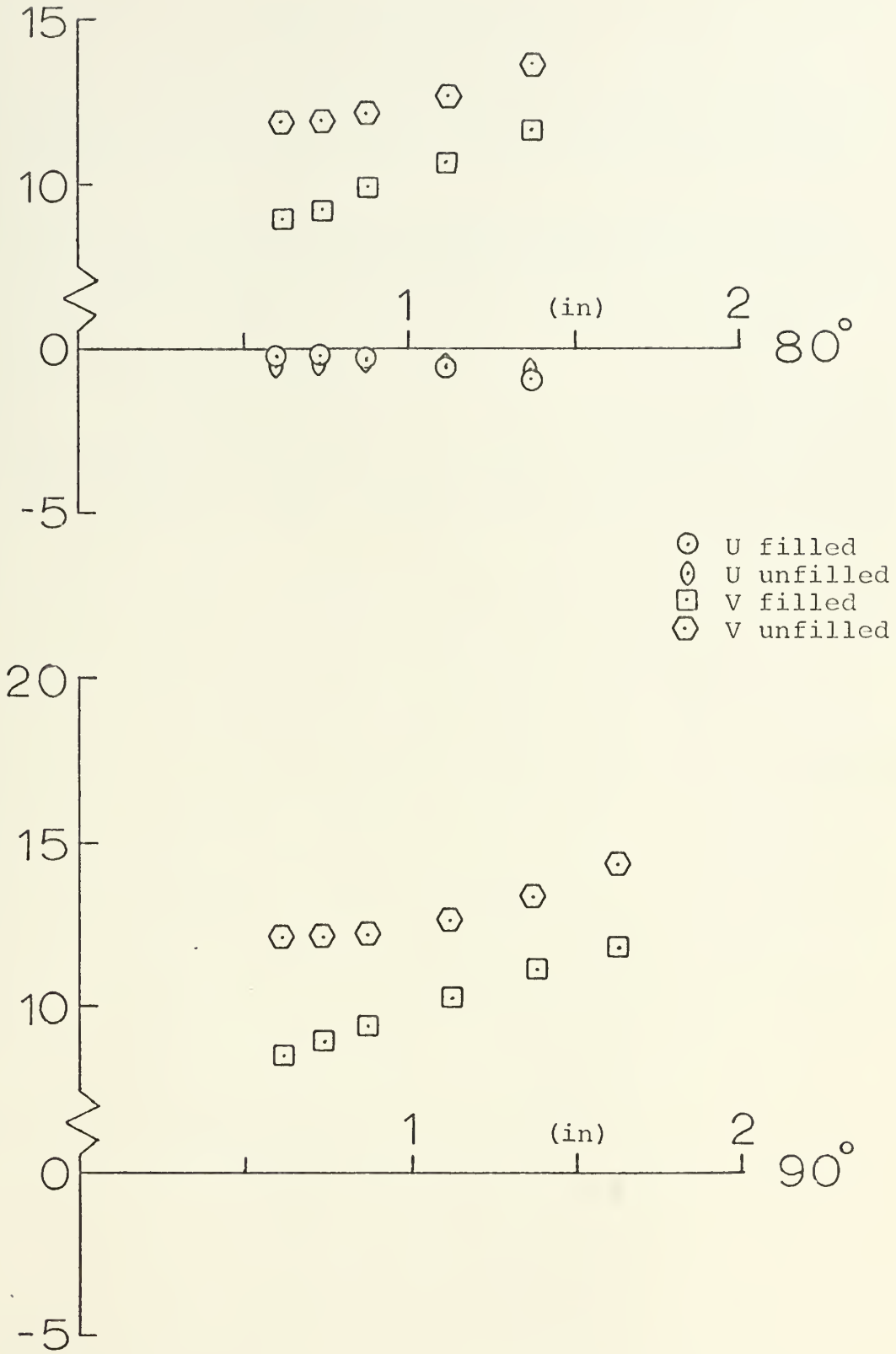

Nondimensional Displacements vs Radial Distance

Figure 31

LIST OF REFERENCES

1. Lindsey, G. H., "Studies Pertaining to Solid Propellant Fracture," NPS-57Li7201lA, Naval Postgraduate School, 1972.

2. Malone, J. P., A Computer Program for the Analysis of Linearly Elastic Plane Stress, Plane Strain Problems, M.S. Thesis, Naval Postgraduate School, Monterey, 1968.

3. Mendelson, A., Plasticity: Theory and Application, MacMillan and Company, 1970.

4. Dhir, S. K. and Sikora, J. P., "An Improved Method for Obtaining the General-displacement Field from a Holographic Interferogram," Experimental Mechanics, Vol. 12, No. 7, pp. 323-327, July 1972.

INITIAL DISTRIBUTION LIST

		No. Copies
1.	Defense Documentation Center Cameron Station Alexandria, Virginia 22314	2
2.	Library, Code 0212 Naval Postgraduate School Monterey, California 93940	2
3.	Professor G. H. Lindsey, Code 57Li Naval Postgraduate School Monterey, California 93940	1
4.	Mr. Alvin R. Hunter, Jr. Lockheed Missiles and Space Company 3251 Hanover Street Palo Alto, California 94304	1
5.	Mr. S. K. Dhir Naval Ship Research and Development Center Bethesda, Maryland 20034	1
6.	LT D. A. Hallwachs 1021 Margaretha Street Two Rivers, Wisconsin 54241	1

UNCLASSIFIED

Security Classification

DOCUMENT CONTROL DATA - R & D

(Security classification of title, body of abstract and indexing annotation must be entered when the overall report is classified)

ORIGINATING ACTIVITY (Corporate author)

Naval Postgraduate School
Monterey, California 93940

2a. REPORT SECURITY CLASSIFICATION

Unclassified

2b. GROUP

REPORT TITLE

An Investigation into Methods of Detecting Dewetted Zones in Solid Rocket Propellants Using Holographic Interferometry

DESCRIPTIVE NOTES (Type of report and, inclusive dates)

Aeronautical Engineer, June 1973

AUTHOR(S) (First name, middle initial, last name)

Donald A. Hallwachs

REPORT DATE	7a. TOTAL NO. OF PAGES	7b. NO. OF REFS
June 1973	67	4

CONTRACT OR GRANT NO.	9a. ORIGINATOR'S REPORT NUMBER(S)
PROJECT NO.	
	9b. OTHER REPORT NO(S) (Any other numbers that may be assigned this report)

DISTRIBUTION STATEMENT

Approved for public release; distribution unlimited.

SUPPLEMENTARY NOTES	12. SPONSORING MILITARY ACTIVITY
	Naval Postgraduate School Monterey, California 93940

ABSTRACT

An investigation was conducted into the possibility of visually detecting a dewetted zone in a solid rocket propellant through the use of holographic interferometry. Techniques used were simple strain, residual strain and time-average holography. As a basis for comparison with experimental data a finite element program was used to model the test samples.

DD FORM 1 NOV 65 1473 (PAGE 1)

S/N 0101-807-6811

UNCLASSIFIED

Security Classification

A-31408

KEY WORDS	LINK A		LINK B		LINK C	
	ROLE	WT	ROLE	WT	ROLE	WT
DEWETTING						
DEWETTING CRITERION						
HOLOGRAPHIC INTERFEROMETRY						
DEWETTED ZONE						

145239

Thesis
H16213 Hallwachs
c.1 An investigation into methods of detecting de-wetted zones in solid rocket propellants using holographic interferom-etry.